240 · 5-18-78

Ch. 82

MLM-2506

MASTER

Mound Facility Activities in Chemical and Physical Research: July-December 1977

May 1, 1978

Monsanto

MOUND FACILITY
Miamisburg, Ohio

operated by
MONSANTO RESEARCH CORPORATION
a subsidiary of Monsanto Company

for the
U. S. DEPARTMENT OF ENERGY

Contract No. EY-76-C-04-0053

DISCLAIMER

PRINTED IN THE UNITED STATES OF AMERICA

Available from
National Technical Information Service
U. S. Department of Commerce
5285 Port Royal Road
Springfield, Virginia 22161
Price: Printed Copy $5.25; Microfiche $3.00

MLM-2506
UC-4 and UC-22

Mound Facility Activities in Chemical and Physical Research: July-December 1977

Issued: May 1, 1978

MOUND FACILITY
Miamisburg, Ohio 45342

operated by
MONSANTO RESEARCH CORPORATION
a subsidiary of Monsanto Company

for the
U. S. DEPARTMENT OF ENERGY

Contract No. EY-76-C-04-0053

Foreword

This report is issued semiannually by Mound Facility. Under the sponsorship of the DOE Division of Basic Energy Sciences, Mound Facility is responsible for producing materials for use in the physical sciences to further the progress of science and technology in the public interest. Additional research activities of related interest under the sponsorship of the Division of Military Application are also reported here.

This report is submitted by W. T. Cave, Director of Nuclear Operations, and R. E. Vallee, Manager of Technology Applications and Development, from contributions prepared by W. M. Rutherford, Science Fellow (Thermal Diffusion); W. L. Taylor, Science Fellow (Gas Dynamics and Cryogenics); G. L. Silver, Senior Research Specialist (Separation Chemistry); R. C. Bowman, Leader, Metal Hydride Research, and from members of the Isotope Separation Section: R. A. Schwind, Isotope Separation Manager; E. D. Michaels, Leader, Isotope Separations Development; W. J. Roos, Leader, Stable Isotopes Production; B. E. Jepson, Leader, Metal Isotope Separation; R. M. Watrous, Leader, Radioisotopes Separation; and V. L. Avona, Leader, Stable Isotope Sales.

These reports are not intended to constitute publication in any sense of the word. Final results will either be submitted for publication in regular professional journals or be published in the form of MLM topical reports.

Previous reports in this series are:

MLM-2168
MLM-2118
MLM-2241
MLM-2296
MLM-2354
MLM-2414
MLM-2450

Contents

$TiFe_{0.79}Mn_{0/15}H_2$ samples. Two $TiCoH_x$ samples were prepared, and low temperature T_1 values were determined. The initial preparation of a single-phase $TiNiH_{1.0}$ was unsuccessful.

Studies of $TiCuH_x$ The proton relaxation times T_1 and T_2 have been measured for $TiCuH_{0.92}$ between 110K and 560K. The low temperature T_1 data yielded a Korringa constant of 41.6 sK. T_2 values above ~460K lead to an approximate hydrogen diffusion activation energy E_a of 0.92 eV.

Diffusion Studies in VH_x Proton T_1 relazation times near the T_1 min were measured at five different resonance frequencies for $VH_{0.50}$ and $VH_{0.76}$. Two approaches will be utilized to obtain the hydrogen diffusion activation energies E_a from the T_1 data. No difference in T_1 values were observed in a $VH_{0.50}$ between heating and cooling cycles during the NMR measurements.

Synthesis of VD_x and VT_x Three vanadium deuteride samples with compositions $VD_{0.53}$, $VD_{0.75}$, and $VD_{1.00}$ were prepared. A sample of $VT_{0.50}$ was synthesized for the first time. X-ray diffraction analyses verified the proper phases for the VD_x and VT_x and provided lattice parameters as well.

Separation Chemistry

Separation Research

Isotope separation

Argon

W. J. Roos

The 13-column argon system continued to produce argon-38 at an intermediate enrichment of 4-5%. This material is being collected for later enrichment to 95%. The system also produced argon-36 at 99.5% enrichment as a by-product.

Carbon

G. E. Stuber, Jr.

A batch of methane containing 67 g of 99% carbon-13 was converted to carbon dioxide. A batch of 99% carbon-13 dioxide was then converted to elemental carbon. A batch of 90% carbon-13 dioxide is being converted to methane for further enrichment to 99% in a thermal diffusion cascade.

Helium-3

W. J. Roos

During this period approximately 600 STP liters of 99.9% helium-3 were produced.

Krypton

G. E. Stuber, Jr.

The nine-column and 19-column thermal diffusion cascades are enriching krypton-86 to 99% in a double cascade arrangement.

A side-stream withdrawal system has been added to the 10-column cascade, and 70% krypton-82 is being produced in a continuous mode.

Neon

G. E. Stuber, Jr.

Batches of neon-20 and neon-22 are being upgraded to product grade in a four-column thermal diffusion system. The material being processed is slightly below product specifications.

Oxygen

G. E. Stuber, Jr.

Fifty-one grams of 37% oxygen-17 water was electrolyzed to produce oxygen gas. Approximately 215 g of 99% oxygen-18 water was electrolyzed to produce oxygen gas. The electrolysis system is presently being modified by the addition of a cold trap in the hydrogen line to prevent the loss of feed water out the hydrogen stream.

Xenon

W. J. Roos

During this period a 19-column thermal diffusion system produced approximately 0.25 STP liter of 40% xenon-124; a 24-column system produced approximately 3.0 STP liters of 5% xenon-124; and an eight-column system produced approximately 4.8 STP liters of 80% xenon-136.

Metal hydride research

Pulse NMR studies

STUDIES OF $TiFeH_x$ AND RELATED SYSTEMS

R. C. Bowman, Jr., A. Attalla, W. E. Tadlock, and D. B. Sullenger

The intermetallic compound TiFe and structurally related titanium alloys, which are

primary candidates for hydrogen energy storage applications, are being investigated by pulse nuclear magnetic resonance (NMR) techniques. The objectives of these studies are to characterize the electronic structure parameters and hydrogen diffusion behavior and to deduce any trends that correlate with the stabilities and hydriding capabilities of these technologically important hydrides.

Although previous NMR studies [1-3] contributed some understanding of the $TiFeH_x$ properties, the tendency of $TiFeH_x$ to form mixed phases and strong inhomogeneous magnetic effects have hindered quantitative interpretation of the experimental results. Consequently, further NMR measurements were performed on two new samples provided by the Materials Research Center of the National Bureau of Standards. The first sample had a nominal composition $Ti_{1.04}Fe_{0.96}H_{1.15}$, and x-ray diffraction measurements at Mound indicated the predominant phase was the tetragonal [a = 3.19(4)Å and c = 8.81(7)Å] β-monohydride with some α-phase TiFe present. The second sample had a nominal composition $Ti_{1.04}Fe_{0.98}H_2$, and only the cubic [a = 6.79(32)Å] γ-dihydride phase was detected by x-ray diffraction. The proton spin-lattice relaxation times (T_1) for the β-phase sample were determined below room temperature and the temperature dependence of T_1^{-1} is shown in Figure 1. These results are in very good agreement with previous [1] NMR measurements on a β-phase $Ti_{0.98}Fe_{1.02}H_{1.03}$ sample prepared at Mound. The sample value of 3.0 sK was obtained for the Korringa constant (T_1T), which is related to the density of electronic states of the Fermi surface, of both samples. Furthermore, the positive deviation of the T_1^{-1} data above 260 K from the linear slope was also seen previously and may be

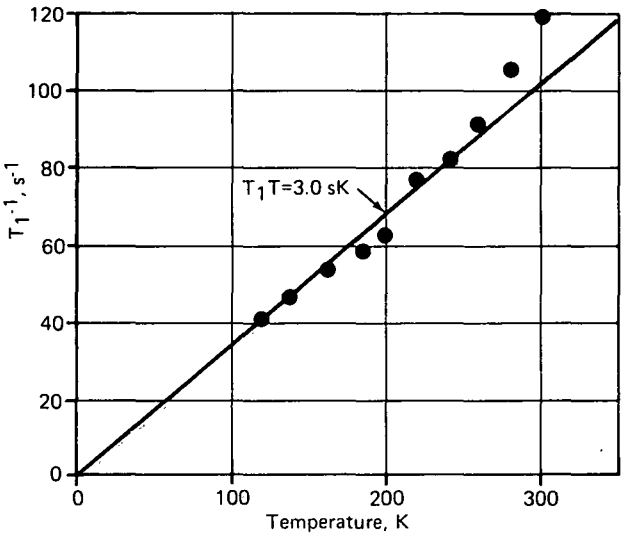

FIGURE 1 - Temperature dependence of proton T_1 for β-phase $Ti_{1.04}Fe_{0.96}H_{1.15}$ sample where the resonance frequency was 34.5 MHz.

indicative of a change in the electronic structure of the β-phase near 260K. Proton spin echoes measurements of the spin-spin relaxation times (T_2') were performed on the γ-phase sample in order to verify the earlier observation [3] that motional narrowing (i.e., T_2' increase by more rapid hydrogen diffusion) begins above ∿390K. As expected, nearly constant T_2' values were obtained up to 400K where a T_2' increase was observed. Unfortunately, the extreme instability of the γ-phase at these elevated temperatures prevented a determination of diffusion activation energy (E_a).

The previous [3] proton spin echo measurements clearly established the hydrogen diffusion in the β-phase $TiFeH_x$ monohydride. Motional narrowing begins at 350(10)K with an E_a of 0.26 eV. An order of magnitude estimate of the hydrogen diffusion constant (D) for the β-monohydride can be

obtained from

$$D = \langle\lambda^2\rangle / 6\tau_c \qquad (1)$$

where $\langle\lambda^2\rangle$ is the mean-squared jump distance (i.e., λ is assumed to be the proton separation distance r_{HH}) and τ_c is the diffusion correlation time. In the limit $\tau_c < M_{2d}^{1/2}$ where M_{2d} is the rigid lattice proton second moment, τ_c obeys

$$\tau_c^{-1} = \gamma_H^2 M_{2d} T_2' . \qquad (2)$$

Because the crystal structure of the β-monohydride has not been determined, r_{HH} (hence, λ) is unknown. However, r_{HH} can be estimated from the approximate expression

$$M_{2d} = C_I \sum_{ij} r_i^{-6} \simeq 8.402 C_I / r_{HH}^6 \qquad (3)$$

where C_I is a constant, the summation is for all protons, and the protons in β-$TiFeH_{1.0}$ are assumed to form a simple cubic unit cell of length r_{HH}. Although the M_{2d} is sensitive to actual arrangements of nuclei in crystal lattices, the approximation in Eq. 3 is valid within a factor of 2-3 for any reasonable structure. The measured $T_2' = 114$ μs at 413K, a calculated $r_{HH} = 3.5$Å from Eq. 3, and a $M_{2d} = 1.60$ G^2 from low temperature spin echo measurements were used to obtain a value of D(413K) = 3×10^{-11} cm^2/s for the β-monohydride. Assuming Arrhenius behavior, $D = D_o \exp(-E_a/kT)$, with $E_a = 0.26$ eV, one obtains a hydrogen diffusion contant for $TiFeH_{1.0}$ of 2×10^{-12} cm^2/s. This value should be reliable within an order of magnitude and compares well with the 300K diffusion constants between 2.2×10^{-12} cm^2/s and 2.7×10^{-13} cm^2/s for TiH_x compositions [4] with x between 1.6 and 1.95. The hydrogen diffusion behavior in β-phase $TiFeH_x$ is also consistent with recent NMR studies of other titanium-based ternary hydrides [5,6]. The kinetics of the charging-discharging of TiFe hydrogen storage systems and inelastic neutron scattering data of Lebsanft, et al. [7] gives an upper limit of $D \lesssim 10^{-8}$ cm^2/s at 343K, which is $\sim 10^3$ times larger than the D implied by the NMR studies. Although NMR gives an order of magnitude estimate for D, the present values are believed to be more reliable than the Lebsanft, et al. upper limit. Extensive microcracking of the TiFe particles occurs during the hydriding process with grain sizes below ~1 μm. In addition, high dislocation densities are also expected which provide additional reaction surfaces. Hence, accurate estimates of the sizes of activated TiFe particles, which are needed to derive D from the charging-discharging times, are difficult. Also, one deals with the α, β, and γ $TiFeH_x$ phases simultaneously in such an analysis. The neutron scattering data [8] give strictly a lower limit of diffusion required for linewidth broadening to be observable and do not yield an actual magnitude for D.

Reilly and Johnson [9] have shown that the pressure-composition behavior of $TiFeH_x$ can be modified in a controlled manner by a partial substitution with other first row transition metals. In particular, the $TiFe_{1-y}Mn_y$ alloy has improved characteristics for hydrogen storage. An alloy of composition $TiFe_{0.79}Mn_{0.15}$ was obtained from Dr. J. Reilly (Brookhaven) and hydrided at NBS to form a γ-phase $TiFe_{0.79}Mn_{0.15}H_2$ sample. Subsequent x-ray analysis at Mound indicated this sample was single-phase dihydride with a cubic lattice parameter of 6.63(3)Å. NMR measurements were performed to determine the proton T_2' and T_1 values. A constant T_2' of 40(1) μs was obtained from spin echo

measurements between 150K and 383K, which indicates an absence of motional narrowing below ∿ 380K in agreement with our data for γ-phase $TiFeH_x$. Hence, the partial substitution of manganese apparently does not significantly increase hydrogen mobility. The effect of manganese on the proton T_1 for the γ-dihydride phase is shown in Figure 2. Although the T_1 temperature dependence is the same for $TiFe_{0.79}Mn H_2$ and $Ti_{1.04}Fe_{0.96}H_{1.98}$ samples, manganese substitution reduces the apparent Korringa constant from 5.5(3) sK to 4.2(5) sK. Hence, manganese does influence the electronic structure of $TiFeH_x$ phase. Further NMR studies of manganese-doped $TiFeH_x$ are planned to establish, more quantitatively, the role of manganese on the electronic structure parameters.

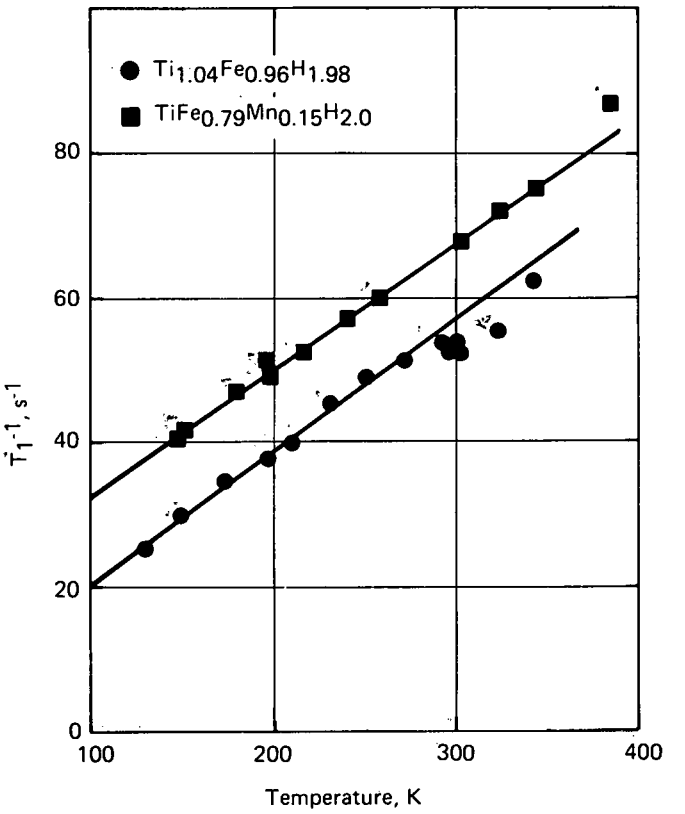

FIGURE 2 - Effect of manganese-substitution on the proton T_1 for the γ-phase $TiFeH_2$ as measured at 34.5 MHz.

In order to extend the NMR studies to other titanium-based ternary hydrides, two compositions of $TiCoH_x$ were synthesized by reacting TiCo (which has the same CsCl crystal structure as TiFe) with high pressure hydrogen gas. Both compositions (i.e., $TiCoH_{1.06}$ and $TiCoH_{1.55}$) were nominally single phase with the tetragonal structure previously found by Yamanaka, et al.[8] for β-phase $TiCoH_x$. Proton T_1 values have been obtained for both compositions and are summarized in Figure 3. Here, as in $TiFeH_x$ the low T_1 values obey the Korringa relation

$$T_1T = C_K. \qquad (4)$$

However, C_K = 35.9 sK and 61.2 sK for $TiCoH_{1.06}$ and $TiCoH_{1.55}$, respectively, and are an order of magnitude larger than the values found for the $TiFeH_x$ phases. Although it would be premature to attempt an interpretation relative to possible differences in the electronic structures of

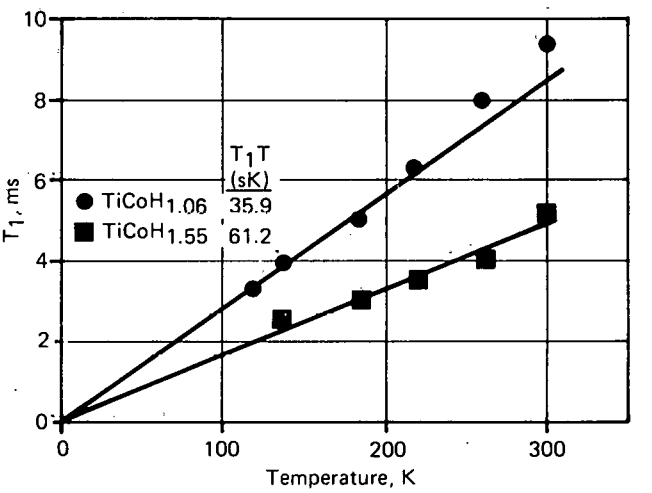

FIGURE 3 - Proton T_1 relaxation times for $TiCoH_x$ when measured at 34.5 MHz.

the $TiFeH_x$ and $TiCoH_x$ phases, such a large difference for presumably similar hydrides is intriguing and may be related to the greatly increased stability [8] of $TiCoH_x$ compared to $TiFeH_x$. However, proton T_1 measurements on other titanium-ternary hydrides are needed before a detailed analysis is attempted.

An attempt to prepare a sample of $TiNiH_{1.0}$ was unsuccessful. Although the reaction between high-pressure hydrogen and TiNi was extremely difficult to initiate, a product of nominal composition $TiNiH_1$ was finally obtained after several days at 200-300°C. However, subsequent x-ray analysis indicated this sample has two major components - the $TiNiH_{1.0}$ phase previously reported by Yamanaka et al. [8] and Buchner et al. [10] and an unidentified phase. Two phases were also found for the unhydrided, but activated TiNi alloy. Since the NMR measurements are extremely difficult to analyze for two-phase systems, this sample had to be rejected. Consequently, the NMR studies will be delayed until this problem is resolved and a single-phase $TiNiH_{1.0}$ can be prepared.

STUDIES OF $TiCuH_x$

R. C. Bowman, Jr

Dr. A. Maeland (Allied Chemical Corporation) recently discovered that b. c. tetragonal γ-phase TiCu will react with hydrogen gas to form a ternary monohydride $TiCuH_{1.0}$ under appropriate conditions (i.e., ∿ 1 atm H_2 pressure and ∿ 150°C). Because of our strong interest in the titanium-ternary hydrides, we obtained a sample of nominal $TiCuH_{0.97}$ from Dr. Maeland. After the relatively large chunks were crushed into a -200-mesh powder, a NMR sample tube was loaded and sealed under a partial helium vacuum. The subsequent gas analysis indicated the actual composition was $TiCuH_{0.92}$ for the powder sample.

Pulse NMR measurements of the proton relaxation times for this $TiCuH_x$ sample were performed at 34.5 MHz between ∿110K and ∿550K. The temperature dependence of T_1^{-1} is presented in Figure 4, and the T_2 values from the high temperature linewidths and spin echoes are given in Figure 5. Since T_1^{-1} increases linearly with temperature below ∿320K, interactions with the conduction electrons clearly dominate the spin-lattice relaxation in this temperature region. A Korringa constant (C_K) of 41.6 sK was deduced from these T_1 data. The increase of T_1^{-1} relative to the predicted Korringa values above ∿450K probably

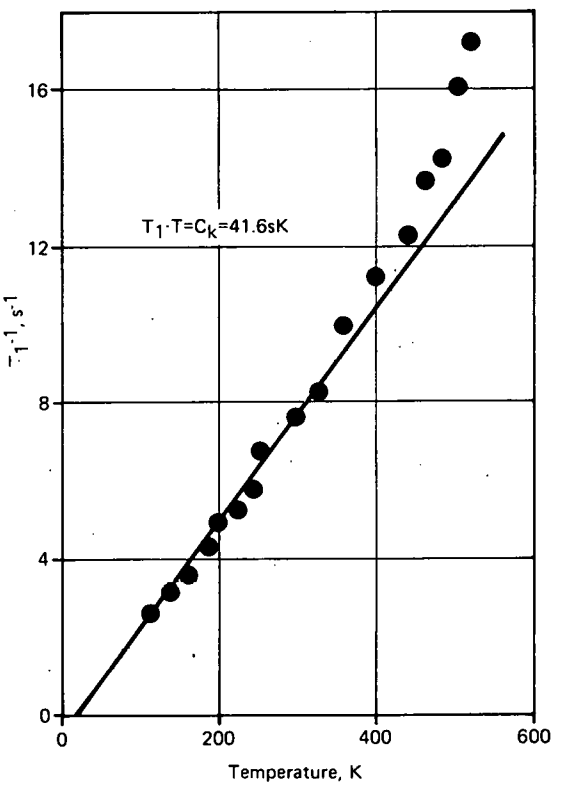

FIGURE 4 - Temperature dependence of proton T_1 for $TiCuH_{0.94}$ for a 34.5 MHz resonance frequency.

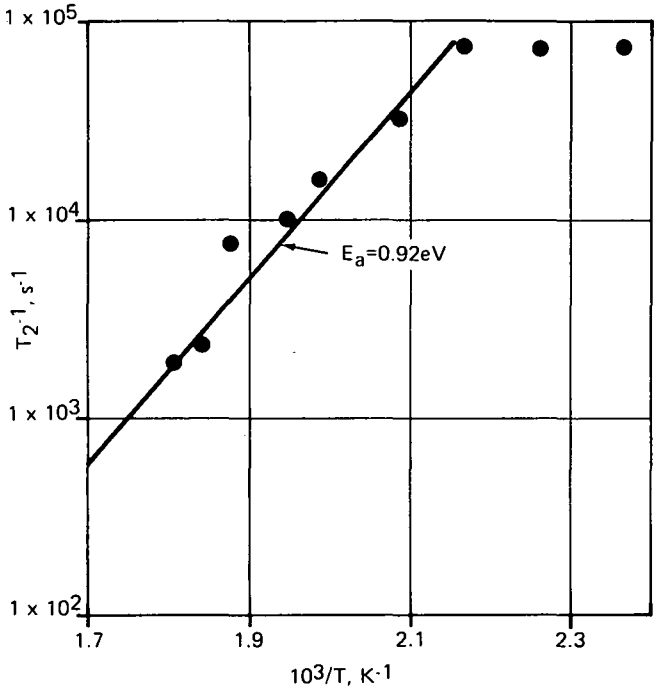

FIGURE 5 - Proton T_2 for $TiCuH_{0.92}$ above 420K.

reflects the influence of hydrogen-diffusion contributions. However, these T_1 measurements are insufficient to permit an estimate of the diffusion activation energy E_a. Figure 5 indicates that motional narrowing of the $TiCuH_x$ proton linewidth does not begin until ∿465K, which is consistant with the T_1 results. An Arrhenius plot of the proton T_2^{-1} values yields a preliminary E_a = 0.92 eV. This E_a for $TiCuH_x$ is much larger than the E_a = 0.5 eV reported [4] for γ-phase TiH_x; however, it is not unreasonable and merely suggests that $TiCuH_x$ may have deeper potentials for the hydrogen diffusion paths.

A second $TiCuH_x$ sample was received in December, 1977, from Dr. Maeland. Similar NMR studies will be performed on this sample too, in an attempt to verify the present observations as well as to permit more detailed analyses of the various parameters.

DIFFUSION STUDIES IN VH_x

R. C. Bowman, Jr., A. Attalla, and B. D. Craft

The VH_x system is being investigated to evaluate the roles of crystal structure, phase transformation, and isotope effects on the hydrogen diffusion mechanisms. A rather comprehensive series of proton T_1 measurements were described in the preceding report of this series [11]. A partial analysis of these results for the b.c.t. β-phase region indicates several unusual features in the apparent hydrogen diffusion behavior for VH_x. Namely, E_a is seen to decrease significantly with hydrogen content, and the diffusion constant has a maximum near $VH_{0.75}$, decreasing at lower and higher stoichiometries. Both of these characteristics are inconsistent with the hydrogen sublattice vacancy model [12] which adequately represents the hydrogen diffusion behavior in several f.c.c. hydrides. However, the diffusion correlation times τ_c deduced from these 34.5 MHz values did not show Arrehenius temperature dependences, as expected, which prevented a more complete analysis. Consequently, the resonance frequency dependences of the proton T_1 values were measured for $VH_{0.50}$ and $VH_{0.76}$. These results are summarized in Figures 6 and 7. Similar procedures to those described previously [11] were used to obtain these T_1 values.

Since the V-H dipolar interactions dominate the diffusion spin-lattice relaxation term T_{1d} near the T_1 minimum, the minimum occurs when

$$\omega_I \tau_c = 2\pi\nu\tau_c = 0.922 \qquad (5)$$

where ν is the resonance frequency in MHz. Consequently, the temperature depencence of the τ_c obtained from the experimental T_1

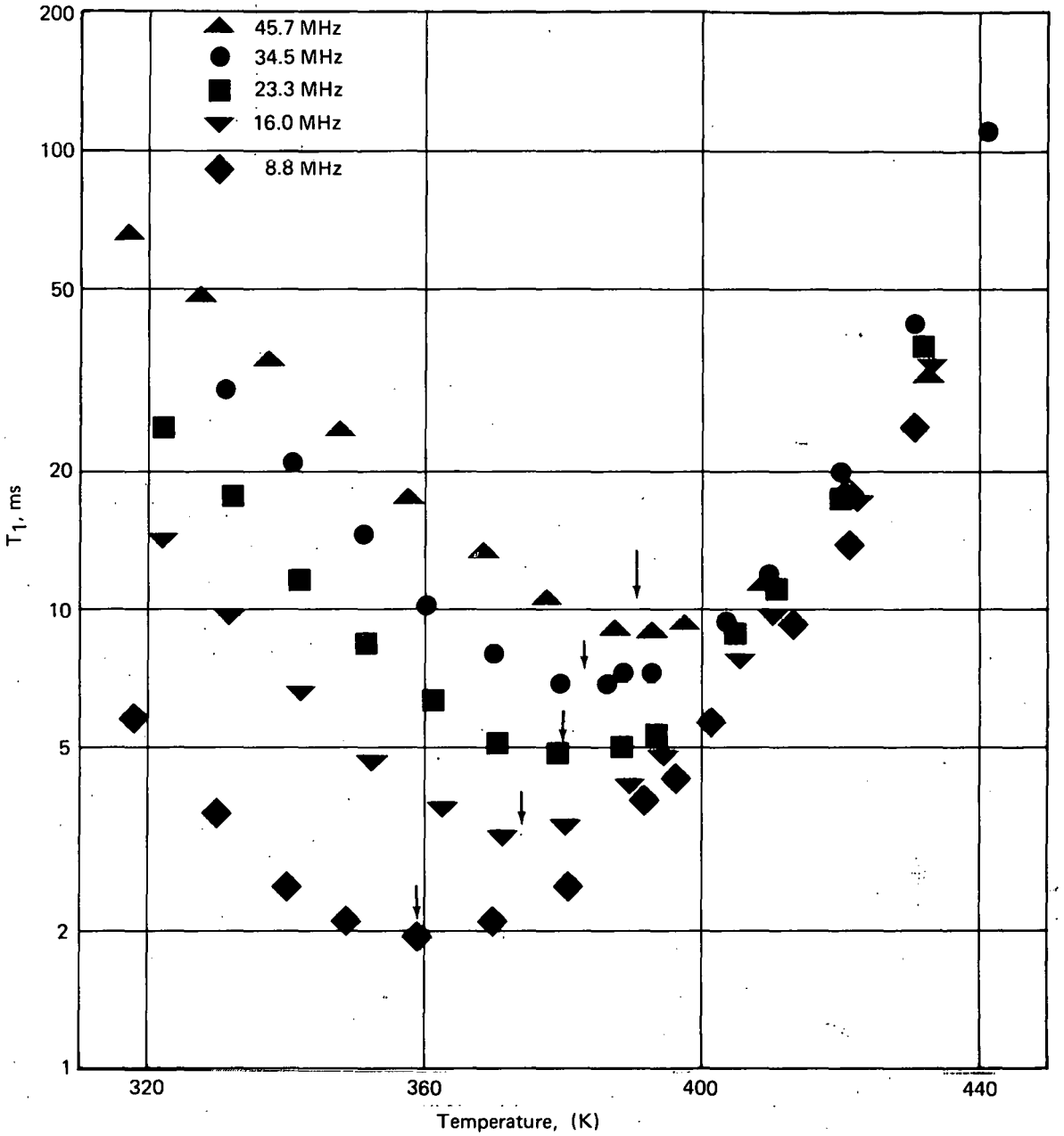

FIGURE 6 - Proton T_1 relaxation times for $VH_{0.50}$.

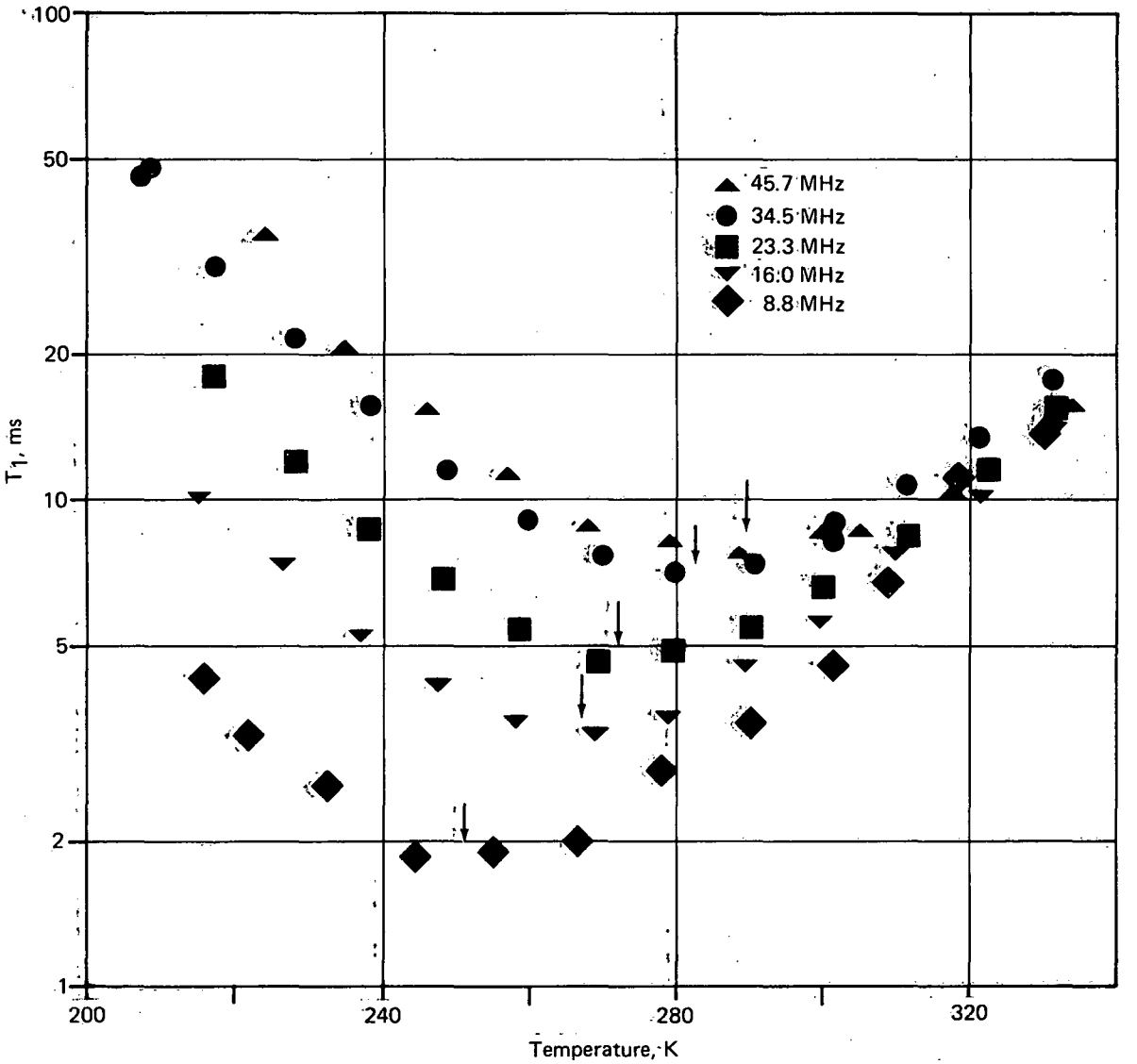

FIGURE 7 - Proton T_1 relaxation times for $VH_{0.76}$.

minimum at each ν can be used to derive the E_a values without explicit model-dependent [11] analyses. Figure 8 presents the Arrhenius plots of the τ_c values obtained at different resonance frequencies for $VH_{0.50}$ and $VH_{0.76}$ as well as previous results [13] for $VH_{0.53}$. The corresponding E_a values, which are included in Figure 8, verify the previous observation that E_a decreases rapidly as the hydrogen content in VH_x increases. The previously described [11] BPP-model calculations were used to determine E_a above and below the T_1 minima from the uncorrected T_1 data in Figures 6 and 7. The frequency dependences and average values of these parameters are summarized in Table 1. At each frequency, different E_a are obtained above and below $T_{1\ min}$ for $VH_{0.50}$ and $VH_{0.76}$, in agreement with our previous [11] analyses on the 34.5 MHz T_1 data. However, the E_a deduced in Figure 8 from the $T_{1\ min}$ are closer to the E_a values derived from the T_1 data above the $T_{1\ min}$. This behavior is suggestive of a far more complex diffusion mechanism in β-phase VH_x than has been found in other hydrides. Consequently, additional data for the proton T_2 and $T_{1\rho}$ relaxation times will be obtained before attempting a more involved interpretation of the hydrogen diffusion processes in VH_x.

Because hysteresis has been observed [14] in the high temperature $\beta \leftrightarrow \alpha$ phase transitions, we were concerned that the proton relaxation times may also show similar behavior near these phase boundaries. Subsequently, the proton T_1 for $VH_{0.50}$ were measured during heating and cooling cycles where the maximum temperature is well into the α-phase. The resulting T_1 values are shown in Figure 9. Clearly, the nearly identical relaxation times that were obtained indicate the processes responsible for T_1 relaxation are relatively insensitive to details in the $\alpha \leftrightarrow \beta$ phase transformation. Hence, subsequent analyses of hydrogen diffusion behavior in VH_x should not be further complicated by any significant variations caused by the manner of crossing this phase boundary.

SYNTHESIS OF VD_x AND VT_x

R. C. Bowman, Jr., W. E. Tadlock, R. L. Yauger, and D. B. Sullenger

Because of the apparent complexity of the diffusion behavior in VH_x, NMR measurements of the proton T_1 relaxation times could not provide comprehensive diffusion mechanisms for VH_x. Because isotope effects in diffusion behavior is a very powerful approach to assess the contributing processes, samples of VD_x and VT_x were prepared for investigating the diffusion isotope effects in these systems. The objective is to gain a more complete understanding of VH_x diffusion mechanisms. In particular, the properties of the tritium nucleus (i.e., I = 1/2 with a magnetic moment 6.7% larger than the proton moment) make NMR studies of the tritium relaxation times in VT_x extremely favorable for quantitatively comparative correlations with the VH_x NMR results. Although VD_x has been prepared and investigated previously [15-19], essentially nothing is known about the properties of VT_x.

The initial step was to prepare a 30-g master batch of VD_x from the same high-purity zone refined-vanadium-metal rod used to synthesize most of the previous VH_x samples. High pressure synthesis techniques resulted in a brittle product with a $VD_{1.00}$ composition. The reactor containing this material was opened in a

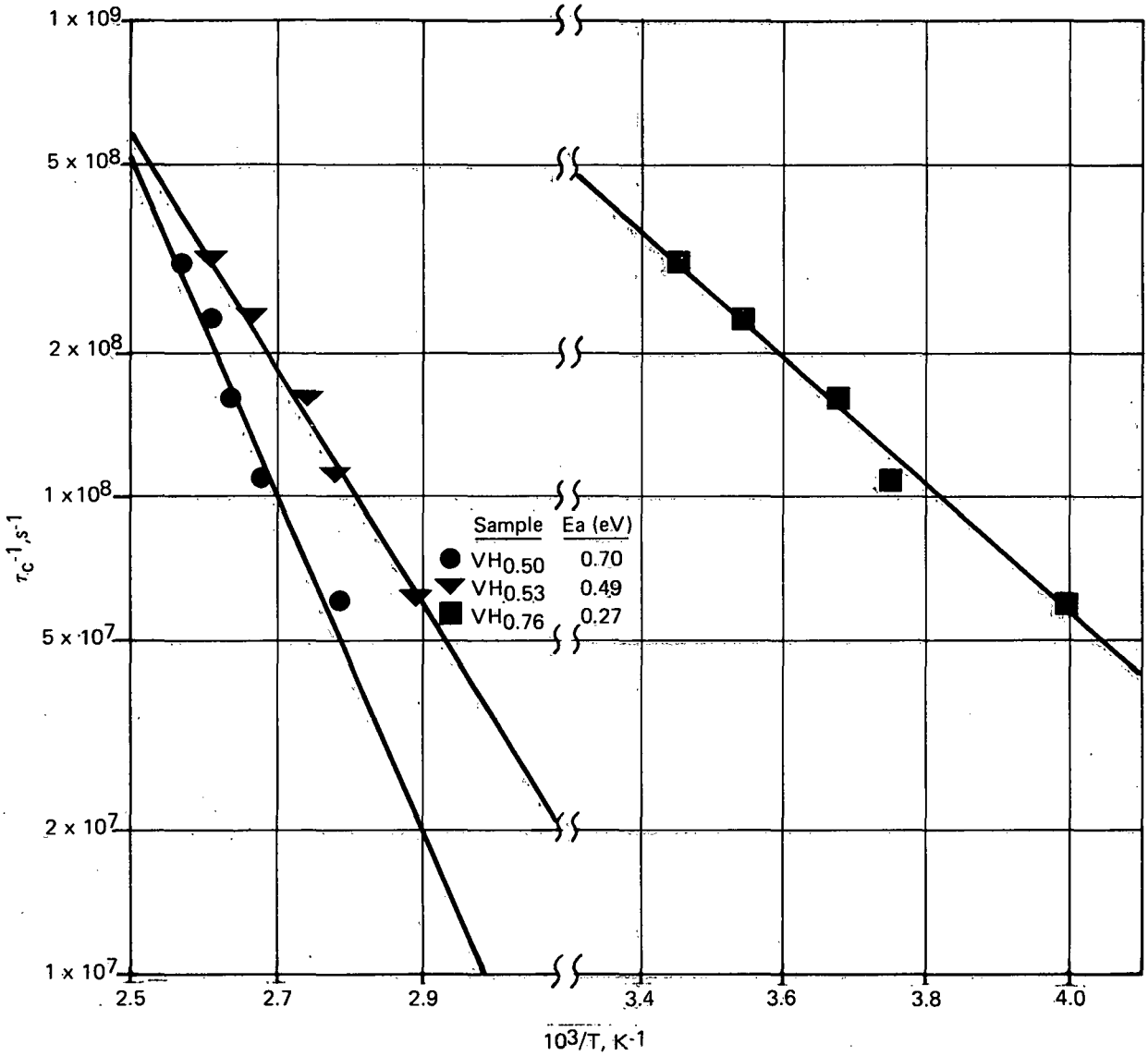

FIGURE 8 - Temperature dependences of τ_c values obtained from T_1 minima at various resonance frequencies.

Table 1 - HYDROGEN DIFFUSION ACTIVATION ENERGIES E_a OBTAINED FROM τ_c VALUES CALCULATED USING BPP-MODEL

	E_a (eV)			
	$VH_{0.50}$		$VH_{0.76}$	
ν (MH_3)	Below T_1 min	Above T_1 min	Below T_1 min	Above T_1 min
8.8	0.42	0.73	0.19	0.27
16.0	0.43	0.67	0.16	0.26
23.3	0.42	0.77	0.18	0.25
34.5	0.41	0.95	0.18	0.27
45.7	0.38	0.66	0.18	0.24
Avg.	0.41	0.76	0.18	0.26

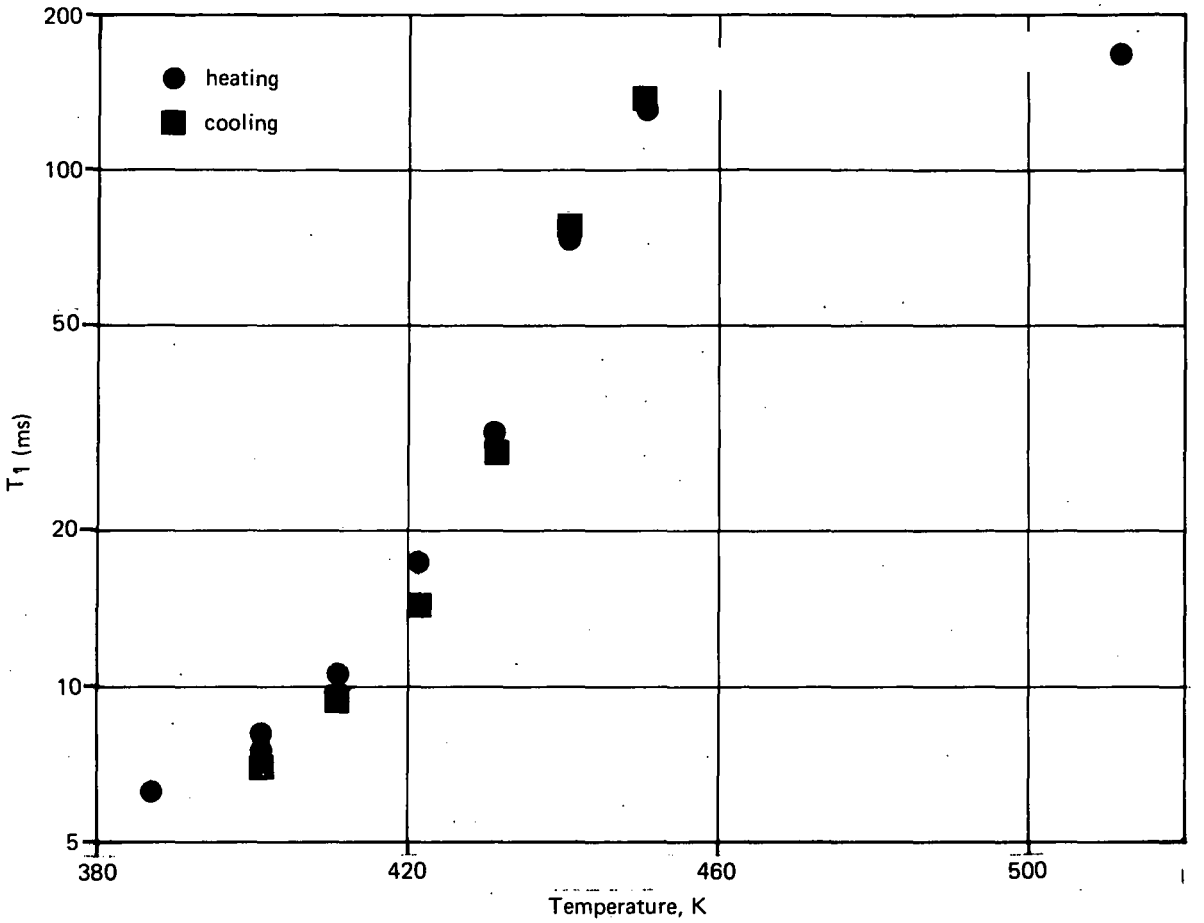

FIGURE 9 - Comparison of the T_1 values obtained during heating and cooling cycles of $VH_{0.50}$.

glovebox system with a high-purity helium-argon atmosphere. The $VD_{1.00}$ was ground to -100 mesh in this boxline. Two 5-g batches of $VD_{0.53}$ and $VD_{0.75}$ were prepared from the $VD_{1.00}$ feed batch. Subsequent x-ray analyses at room temperature determined the composition of the VD_x materials. In agreement with the previous work of Hardcastle and Gibb [15] and others [17,18], $VD_{0.53}$ consisted mainly of b.c.t. β-phase, $VD_{0.75}$ contained only b.c.c. α'-phase, and $VD_{1.00}$ was mainly α'-phase with evidence of the presence of some γ-phase VD_2. A NMR sample tube was loaded and sealed for each VD_x composition.

The first VT_x prepareation was a 9-g batch of nominal $VT_{0.5}$. Calorimetry and volumetric-mass spectrometry analyses of this product gave an initial composition of $VT_{0.50}$. The x-ray diffraction analysis of $VT_{0.50}$ indicated a b.c.t. structure with a_o = 2.990(12)Å, c_o = 3.222(14)Å, and c_o/a_o = 1.078. These lattice parameters are in excellent agreement with the results predicted from β-phase $VH_{0.50}$ and $VD_{0.50}$. Hence, the present $VT_{0.50}$ sample should be directly comparable to the $VH_{0.50}$ currently being investigated. Three NMR sample tubes were loaded with measured quantities of $VT_{0.50}$ and torch sealed after evacuation. NMR measurements of the tritium relaxation times have begun.

Separation chemistry

Equilibrium calculations for environmental plutonium

G. L. Silver

Several years ago a method for estimating the distribution of plutonium oxidation states (including plutonium(IV) polymer) in aquatic systems was suggested. This method depended upon the measurement of the aquatic oxidation-reduction potential and pH, as these values may be combined with a statement of mass conservation for plutonium ions to determine the proportional distribution of these ions [20,21]. In order to account for complexation effects, it was suggested that use be made of plutonium ion alpha coefficients. These alpha coefficients probably do not need to be known with much accuracy [22], and so it was suggested that the ratio of the solubility of a salt of an ion like one of the plutonium ions (e.g., Nd^{3+} for Pu^{3+}) be measured in environmental water as well as in distilled water of about the same ionic strength as the natural water. The ratio of these solubilities may be used to estimate the plutonium ion alpha coefficients, since the definition of an alpha coefficient is the total concentration of an ionic species (including complexes) divided by the concentration of uncomplexed ionic species [23]. This method also avoids criticisms applied to alpha coefficient determinations by purely computational techniques [24].

With a measure of solution pH, oxidation-reduction potential, and complexation ability for the various plutonium ions (as determined by estimating the plutonium ion alpha coefficients), the equilibrium distribution of plutonium valence states may be approximated [21]. Since these calculations are applicable only to equilibrium circumstances, however, and since there is usually no information on whether or not the plutonium in an aquatic system is at equilibrium, it is reasonable to ask what useful purpose could be served by performing the experiments and calculations outlined above.

More than one point may be offered to the above objection. First of all, this approach is new and seems never to have been tried before. In a field of study still characterized by uncertainty and active interest, as is the study of plutonium in the environment, new ideas are often needed. It may be discovered that the application of equilibrium calculations to aquatic systems yields new insights which might not otherwise have been as readily obtained.

The approach outlined above yields information on equilibrium systems only. Since an aquatic system cannot easily be proved to be at equilibrium nor to contain plutonium which is at equilibrium (or even in steady state with a nonequilibrium aquatic system), it may be argued that the new approach is therefore not worth the effort. But to this objection may be raised the following question, "What constitutes useful information in the study of environmental plutonium?" Suppose, for example, that all of the above measurements had been obtained on a particular aquatic system, and suppose that these measurements indicate an equilibrium distribution of plutonium oxidation states comprised of 25% Pu(III), 0.01% Pu(IV), 75% Pu(V), and 0.01% Pu(VI). Suppose further that the real (nonequilibrium) distribution of soluble plutonium species in the aquatic system were about 15% Pu(III), 0.05% Pu(IV), 84% Pu(V), and 1% Pu(VI). Then it may be

said that the experimental work or the calculations are somewhere in error, and that the conclusions are wrong. But an approximation which is as close to the actual circumstances as the approximation described above is an achievement not commonplace in environmental plutonium studies. Although the procedure herein described for estimating plutonium oxidation state distributions may not give a strictly correct answer, the answer may nevertheless be a useful and interesting guide to the chemistry of plutonium in the environment and to which plutonium oxidation states are likely to be predominant or most important. Moreover, chemical reactions proceed in the direction of equilibrium. Even if the plutonium is not at equilibrium in the environmental system, it may be interesting and useful to know in which direction future valence state adjustments may proceed.

The calculation of the equilibrium valence state distribution of dissolved plutonium does not depend upon the absolute solubility of the plutonium. The absolute concentrations of plutonium species in an aquatic environment do, however, depend upon the solubility of the insoluble form of the plutonium in the aquatic system. Polzer used a solubility product applied to plutonium dioxide in order to approximate the absolute concentration of tetravalent plutonium in an aquatic system [25], a procedure later criticized by Patterson, Nelson, and Matlack [26]. In order to demonstrate equilibrium calculations, Silver used a solubility product applied to plutonium polymer (or dispersed hydrous plutonium(IV) oxide) which he estimated from free energy considerations related to the formation of plutonium(IV) polymer [20]. But there is no reason to believe that the value used by Silver is any better than other popular values of the solubility product of plutonium(IV) hydroxide. Experimental determinations of the solubility product of tetravalent plutonium hydroxide differ by many powers of 10, and there seems to be no way of assessing what numerical value for this solubility product is most appropriate for environmental circumstances [27]. However, whether the formula $Pu(OH)_4$ or PuO_2 is used for calculation purposes may be academic, since the algebra of computation is unaffected:

$$Pu(OH)_4 = Pu^{4+} + 4OH^- \qquad (1)$$

$$PuO_2 + 2HOH = Pu^{4+} + 4OH^- \qquad (2)$$

The solubility product of the plutonium in either equation above may be taken as the product of the concentration of the tetravalent plutonium cation and the fourth power of the hydroxyl ion concentration. As mentioned above, the principal point of uncertainty, at least as far as calculations related to dissolved plutonium species are concerned, is the numerical value to be used for the solubility product.

In the study of environmental systems, obtaining reliable pH values and potential values are important if equilibrium calculations are to be useful. But obtaining reliable and meaningful pH and Eh values may not be an easy task. Garrels and Christ have described some of the difficulties in measuring acidity and redox values in aquatic environments, and particularly warn against misleading potential values which may be obtained by use of the platinum electrode [28].

Solution of the plutonium (N,H) equation

G. L. Silver

The advent of inexpensive, programmable pocket calculators promises to make the numerical solution of tedious polymonial equations a commplace operation. Standard numerical techniques for solving polynomial equations, such as the bisection or modified Regula-Falsi techniques, can be adapted to programmable pocket calculators, but may require more calculator memory than the user cares to sacrifice. Some standard techniques such as the bisection method may also be quite time consuming. For reasons such as these, a series solution of a polynomial equation is appealing, since techniques may be found for hastening the convergence of an infinite series [29]. Silver examined one series (a series based on the theorem of Lagrange) for solving polynomial equations and remarked some of the difficulties which may accompany polynomial solution by infinite series [30].

Let the plutonium (N,H) polynomial be reduced to the following standard form:

$$M^3 - bM + a = 0 \qquad (1)$$

so that

$$1/b = M/(M^3 + a) \qquad (2)$$

If the division is executed in the order so indicated, the following series results

$$1/b = 1/M^2 - a/M^5 + a^2/M^8 - a^3/M^{11} + \ldots \qquad (3)$$

The square root of both sides of series 3 may be extracted so that

$$\sqrt{1/b} = (1/M)\,g(1/M) \qquad (4)$$

where g(1/M) is the square root of the series

$$1 - a/M^3 + a^2/M^6 - a^3/M^9 + \ldots \qquad (5)$$

Let Z = 1/M so that Eq. 4 becomes

$$\sqrt{1/b} = (Z)g(Z) = f(Z) \qquad (6)$$

But Eq. 6 may be expanded by a Maclaurin series expansion, and this Maclaurin series expansion may be reverted to give another series:

$$Z = \sqrt{1/b} + (a/2)\,(\sqrt{1/b})^4 + \ldots \qquad (7)$$

Series 7 may be used to evaluate the root of the plutonium (N,H) equation, although the development of successive series terms becomes increasingly difficult and tedious.

Series 7 has another application. Many programmable pocket calculators are equipped with prepared routines for solving simple polynomial equations. The Hewlett Packard Model 67 programmable pocket calculator is equipped with a program called "Calculus and Roots of f(x)". (This program is program #11 of the standard calculator programs.) Although this program will solve simple polynomial equations, the user must supply the routine with an initial guess for the root of the polynomial. Users of this program are warned that a bad guess may result in a long execution time or in a machine error. Series 7, even when taken only to two terms, may provide a satisfactory initial guess for the Hewlett Packard standard program. This initial guess may be obtained either by summing the two given terms as indicated, and then taking the reciprocal of this sum, or by calculating the average of the first term and the sum of the first two terms, and taking the reciprocal of this average.

There are many other methods for calculating the roots of a polynomial equation by means of a series. Some of these methods are uncomplicated [31], but some are so arcane and tedious as to render them impractical for the user of the pocket calculator [32]. (For example, Merriman and Woodward state that the cubic equation

$$Y^3 + 3BY + 2C = 0 \qquad (8)$$

can be solved by the series

$$Y = 2(-C)^{1/3}(1-(2/2)(R) - \frac{(2)(5)(8)}{(2)(3)(4)}(R^2) - \frac{(2)(5)(8)(11)(14)}{(2)(3)(4)(5)(6)}(R^3) - \ldots \qquad (9)$$

where $R = (B^3 + C^2)/(3C^2))$. (10)

They remark, however, that this solution is of use in comparatively few cases [33].

Finding simple methods for solving the polynomial equations which arise in the plutonium chemistry is only one of many interesting problems in plutonium chemistry deserving further attention. Examples of other such problems have been given elsewhere [34-37].

Acknowledgement: The author wishes to thank J. J. Bastian of the Wright State University Mathematics Department for his assistance with this work.

Protactinium-231 and thorium-230

M. R. Hertz and P. E. Figgins

Mound Laboratory is recovering thorium-230 and protactinium-231 from a uranium mill by-product known as "Cotter Concentrate" and ships the products to Isotope Sales at Oak Ridge National Laboratory (ORNL). Previous reports in this series contain detailed descriptions of the origin and character of the Cotter Concentrate and the facilities and development of the current recovery and purification processes. Briefly, the process consists of leaching 20-25 liter batches of the solids with hot, concentrated HNO_3, diluting, and filtering out the insoluble residue. Uranium is removed from the 90-liter batches of the filtrate by liquid-liquid solvent extraction with 10% DSBPP/CCl_4 (di-sec-butylphenylphosphonate in carbon tetrachloride) after which the uranium is stripped from the organic with 0.005 M HNO_3. Thorium is extracted from the filtrate by multiple contacts with 0.1 M TOPO/CCl_4 (tri-n-octylphosphine oxide in carbon tetrachloride) with each contact followed by a 0.3 M H_2SO_4 strip. After the thorium has been removed from the filtrate, further contacts with TOPO/CCl_4, each followed by an 0.5 M oxalic acid strip, results in recovery of the protactinium. Uranium strip solutions are precipitated with ammonia and the precipitate is collected for eventual return to the uranium processor. The thorium strip solutions are purified by oxalate precipitation and calcined to the oxide. Protactinium strip solutions are concentrated by evaporation after which they are processed by the following sequence of operations:

The bulk of the impurities are removed during a TOPO/DEHPA extraction from 7 M HNO_3. The protactinium is stripped with dilute HF, and the HF removed by two hydroxide precipitations.

Additional purification is achieved by phosphate precipitation from a 2 M HCl/0.5 M oxalic medium [38-39]. Careful control of the precipitation conditions is required, and recycle precipitations

are usually necessary. The phosphate precipitate is dissolved easily by treatment with hot caustic solution.

When the solution has been reduced to a suitably small volume, it is dissolved in H_2SO_4 and HCl, and the protactinium is extracted with DIBC and then stripped with oxalic acid. Protactinium is further concentrated and purified by heating and hydrolyzing the oxalic strip solution.

Final purification and preparation of the protactinium for shipment usually includes one or more cycles of recrystallization from concentrated H_2SO_4, followed by hydroxide precipitation, drying, calcining, and packaging.

Numerous problems are recognized in this protactinium purification procedure and are being worked on. The process is too long, and some of the separations depend upon exact control of conditions. Planned improvements are to increase the amount of protactinium in each batch to improve the efficiency, and samples are being analyzed by emission spectrographic analysis to determine what impurities are causing the problems. Alternate conditions and alternate separation methods will be tested.

A batch of protactinium, totalling 220 mg, was purified by this method and shipped to Isotope Sales at ORNL. Approximately 150 mg of protactinium, recovered from Cotter Concentrate, has been evaporated and is awaiting TOPO/DEHPA extraction. Another 50 mg of recycle material is being processed.

Since the last report, nine additional batches of Cotter Concentrate have been processed from Drums No. 172 and 201.

A shipment of 35,577 mg of purified thorium-230 was made to Isotope Sales at ORNL, completing the FY-1977 quota. Thorium purity was equal to that of previous shipments. An additional 17,085 mg is on hand from recent production.

Thorium-229

W. R. Deal

A total of 13.4 mg of thorium-229 has been extracted, purified, and shipped to Isotope Sales, ORNL, since the last semiannual report. This material was separated from a 207-g batch of high-purity UF_4. Thorium-229 was 37.79% of the total thorium, determined from mass spectrographic analysis.

The last batch of high-purity UF_4 is being processed. This batch contains approximately 15 mg of thorium-229 in 186 g of uranium-233.

The contract for construction of a liquid uranium-233 solution storage facility has been signed, but construction has not yet begun. Contract terms specify 180 days for completion. The calibration and testing are expected to be completed by the end of FY-1978. Initial dissolution of uranium-233 and filling of the tanks are expected to be under way in FY-1979.

Uranium-234

P. L. Keister and P. E. Figgins

Mound Facility has been separating and recovering high isotopic purity uranium-234 from aged plutonium-238 materials for several years. The general chemical procedures were described previously [40].

INITIAL SEPARATION

The intial separation of uranium from plutonium "cow" A10-02 by oxalate precipitation of the plutonium was completed this period. This was the second cycle of separation for A10-02, which contained 33.2 g of plutonium-238 with an estimated 1.3 g of uranium-234. The A10-02 "cow" was dissolved in hot, concentrated HNO_3 containing 0.05-0.1M HF. After the solution was adjusted to 2M HNO_3 using NH_4OH, the plutonium was precipitated as the oxalate with dimethyloxalate using H_2O_2 as reductant for plutonium. The oxalate precipitate was collected by vacuum filtration and combined with the oxalate precipitate of the initial separation from "cow" A10-01 [41]. The combined precipitates were designated B10-0, calcined to the oxide at 900°C, and returned to plutonium "cow" storage. The uranium-rich oxalate filtrates were combined and evaporated to concentrate the volume and destroy the oxalate. The concentrated filtrate was designated B10-filtrate and held for the intermediate separation step. This completed the initial separation of an estimated 7.7 g of uranium-234 and 194.1 g of plutonium-238 "cow" material selected to meet a part of the FY-1977 production goal of uranium-234 with 99+% isotopic purity.

The uranium-rich C14 and A18-filtrates [41] were combined and designated C14/A18-filtrate for intermediate processing. This filtrate was salted to 1.6M with $Al(NO_3)_3$ and adjusted to 0.3M HNO_3 using NH_4OH. Hydroxylamine nitrate was added as a reductant for plutonium. The salted feed was loaded onto a column of Dowex 1 x 4 anion exchange resin (nitrate form) which had been preconditioned with 1.6M $Al(NO_3)_3$/0.3M HNO_3. The column was washed with 1.6M $Al(NO_3)_3$/0.3M HNO_3, and the uranium was eluted with 7M HNO_3. Finally, the plutonium was eluted with 0.35M HNO_3 containing hydroxylamine nitrate as reductant for plutonium. Alpha pulse height analysis indicated a uranium fraction suitable for the final separation with 4.16 g of uranium-234 and 19 mg of plutonium-238.

INTERMEDIATE PROCESSING

B10-Filtrate Intermediate processing of B10-filtrate was completed this period, but not without some problems. During loading of the salted feed, there was an excessive amount of gas formation on the resin column with a considerable reduction in flow rate. These problems persisted through the washing and elutions. Fine, white solids were observed in the resin column and in portions of effluents from the column. Alpha pulse height analysis indicated a uranium fraction of 3 g of uranium-234 and 216 mg of plutonium-238. This was three to four times more plutonium-238 than desirable for proceeding to the final separation step. At this point, possible contributions to the problems and results encountered were identified as higher than normal plutonium-238 content (1.5 g) in the feed and the fact that this material originated from "cow" material with a significant zirconium impurity.

Before B10 was reprocessed, the intermediate processing of B16-filtrate [41] was completed. During the loading of the salted feed, the flow rate quickly dropped to almost nothing. It was probable that the fine, white solids observed during the previous operation had "plugged" the column. The resin was transferred to a beaker, and the anion exchange was completed by batch contact with vacuum filtration

between fractions. Alpha pulse height analysis indicated a uranium fraction suitable for final separation of 1.05 g of uranium-234 and 19 mg of plutonium-238.

The uranium fraction from the unsuccessful intermediate processing of B10 was prepared for a rerun using fresh resin. For this run, the uranium fraction was prepared as feed by evaporation to a minimum volume and adjustment to 7M HNO_3. The intent was to load only plutonium and to wash the resin with 7M HNO_3 to remove the uranium. The column was preconditioned with 7M HNO_3, the feed was loaded, the uranium was removed with 7M HNO_3 wash, and the plutonium was eluted with 0.35M HNO_3 containing hydroxylamine nitrate as reductant for plutonium. Alpha pulse height analysis indicated the uranium fraction from the rerun still contained 200 mg of plutonium-238. Apparently, proper valence adjustment of the plutonium had not been made. The rerun was repeated with hydroxylamine chloride added as a reductant to the feed as it was prepared. This resulted in a slight improvement. Alpha pulse height analysis indicated a uranium fraction with 170 mg of plutonium-238 and still not suitable for final separation.

For a final attempt at intermediate separation, the B10 uranium fraction was concentrated by evaporation with addition of oxalic acid and hydrazine dihydrochloride as reductants for plutonium. The uranium and plutonium were precipitated with NH_4OH, and the precipitate was dissolved in 1.6M $Al(NO_3)_3$/0.3M HNO_3. Hydroxylamine nitrate was added to this feed just prior to a standard anion exchange in nitrate media. Alpha pulse height analysis indicated 19 mg of plutonium-238 in the 3 g of uranium-234 fraction which was suitable for final separation. This completed the intermediate processing of material expected to produce a uranium-234 product of 99+% isotopic purity to meet part of the FY-1977 production goal.

A15-Filtrate The special initial processing of batch A15 has been described previously [42]. Some of this material was processed to a final uranium-234 product and identified as having 96% isotopic purity. A portion of this material, designated A15-FILT-B and containing an estimated 7.6 g of uranium-234 with 0.5 g of plutonium-238, was processed this period to meet a part of the FY-1977 production goal. This material was selected to be used in a solvent extraction with DSBPP (di-sec-butylphenylphosphonate) as an option to anion exchange in nitrate media for the intermediate separation step.

In the thorium-229 project at Mound, DSBPP has been shown to be useful in separating and purifying uranium. The literature [43,44] indicates that Pu(IV) is extracted by DSBPP, but not quite as well as uranium is. Although data are not given, it was expected that Pu(VI) would be extracted moderately well, and Pu(III) would not be extracted; preliminary experiments tended to confirm this. A semiautomatic solvent extraction system, similar to one described previously [45], was assembled. The extractant was 10% DSBPP in tetrachloroethylene (heavy phase), and the feed solution (light phase) was approximately 2M in HNO_3. Approximately 900 ml of feed solution was agitated with 200 ml of organic (magnetic stirrer); then from a settling zone, the organic was transferred by an air lift to a stripping cell. In the stripping cell, another magnetic stirrer contacted 200 ml of

organic with 200 ml of water or dilute (0.005 M) HNO_3. A weir controlled the flow of stripped organic back to the extraction cell. Strip solution was added by gravity and overflowed to a storage bottle.

The A15-FILT-B solution was diluted 1:2 with 0.35 M HNO_3 (est. U = 1.3 g/liter, Pu = 0.01 g/liter, HNO_3 = 2 M) and extracted in six batches, for periods of 3 to 6 hr each. Approximately 1000 ml of strip solution was used for each batch, but some strip solutions were recycled. The combined strip solutions were concentrated by evaporation and precipitation, then adjusted to 2 M HNO_3 for a second cycle of extraction.

During the first-cycle extraction, no adjustment of plutonium valence was performed, and it was planned to extract all the plutonium so the raffinates could be discarded. For the second cycle, hydroxylamine nitrate was added to the feed solution prior to and during the extraction to hold the plutonium as Pu(III), but otherwise the procedure was the same.

During these extractions, samples were taken and counted on the LEPS (low energy photon system). This technique uses gamma peaks at 43, 53, and 59 keV as semiquantitative measures of uranium-234, plutonium-238, and americium-241 respectively. The strong 59 keV americium-241 peak masked the 53 keV uranium-234 peak in the feed solution, and it was not possible to determine urnaium recovery. However, the americium separation was excellent, and the uranium-234 peak was used in evaluating the strip solutions and in the second cycle. The data indicated that most (90+%) of the plutonium was extracting in the first cycle, and the extraction of uranium should be even better. However, in the second cycle, when the plutonium should have been in the form of nonextractable Pu(III), at least half of the plutonium accompanied the uranium. This was subsequently attributed to incomplete reduction of the plutonium, and in future runs, more strenuous reduction techniques will be used. At this point, the solvent extraction procedure seems to offer potential advantages in the intermediate step. This particular type of solution had been difficult to handle in the anion exchange procedure, and these difficulties were avoided. The semi-automatic nature of the extraction means less attention is required, but the total time required is comparable to the anion exchange.

Since the solvent extraction of A15-FILT-B did not achieve the desired plutonium separation to replace anion exchange as the intermediate separation step, the strip and some raffinate solutions from the second cycle were prepared for the anion exchange in nitrate media. The solutions were concentrated by evaporation with addition of oxalic acid and hydrazine dihydrochloride as reductants for plutonium. The uranium and plutonium were precipitated from the concentrated solution with NaOH and redissolved in 1.6M $Al(NO_3)_3$/0.3M HNO_3. Hydroxylamine nitrate was added to this feed just prior to a standard anion exchange in nitrate media. Alpha pulse height analysis indicated a uranium fraction suitable for final separation of 8.04 g of uranium-234 and 6 mg of plutonium-238. This completed the intermediate processing of material which would produce a uranium-234 product of 96% isotopic purity to meet part of the FY-1977 production goal.

FINAL PROCESSING

The final processing of recycled material from final separation of product A13-3 [47] was completed this period. Several chloride solutions with recoverable uranium-234 (99.08% isotopic purity) were combined and adjusted to 9M HCl for final processing by anion exchange in chloride media. The prepared A13 recycle feed was loaded onto a column of Dowex 1 x 4 anion exchange resin (chloride form) which had been preconditioned with 9M HCl. The plutonium was eluted with 9M HCl/0.05M NH_4I, and the column was washed with 9M HCl. A neptunium fraction was eluted with 4M HCl, and the uranium was eluted with 0.5M HCl. Alpha pulse height analysis indicated a uranium fraction suitable for final product preparation of 2.5 g of uranium-234 and less than 0.01 mg of plutonium-238.

Uranium fractions from the intermediate processing of A10-P [41], C14/A18, B10, and B16 were prepared for final processing by conversion from nitrate to chloride form. Conversion was accomplished by double precipitation with NaOH and subsequent dissolution in 9M HCl.

The chloride forms of uranium fractions A10-P and one-half of C14/A18 were combined, and final processing by anion exchange in chloride media was completed. Alpha pulse height analysis indicated a uranium fraction suitable for final product preparation of 5.2 g of uranium-234 and less than 0.01 mg of plutonium-238.

The chloride forms of uranium fractions B10 and B16 and the final one-half of C14/A18 were combined and final processing was completed. During loading of the feed, the flow rate dropped to almost nothing. There were some white solids observed collecting on the resin. The resin was transferred to a beaker, and the anion exchange was completed by batch contact with vacuum filtration between fractions. Alpha pulse height analysis indicated a uranium fraction suitable for final product preapartion of 4.75 g of uranium-234 and 0.025 mg of plutonium-238.

The uranium fractions from the preceding three final processing operations were combined and designated final product 77-1. This product was expected to have an isotopic purity of 99+%. The uranium was precipitated with NH_4OH, and the precipitate was calcined to the oxide at 900°C. The total oxide weight of product 77-1 was 15.250 g. Alpha pulse height data indicated 13.8 ppm of uranium-232 and 5.3 ppm of plutonium-238. Based on alpha pulse height data and proportional counting, the uranium-234 weight was calculated as 12.363 g. Mass analysis indicated product 77-1 had an isotopic purity of 99.081%.

The uranium fraction from the intermediate processing of A15-FILT-B was prepared for final processing by conversion from nitrate to chloride form and adjusted to 9M HCl. Recycled material from final separation of product A15-1 [42] (96% isotopic purity) was also prepared for final processing with several chloride solutions containing recoverable uranium-234 being adjusted to 9M HCl. The final processing for all this A15 material was completed in two standard anion exchanges in chloride media. The column had been charged with fresh resin. Alpha pulse height analysis indicated uranium fractions suitable for final product preparation with totals of 7.85 g of uranium-234 and 0.026 mg of plutonium-238.

The two A15 uranium fractions from final processing were combined and designated

final product A15-2. This material had already been identified as having an isotopic purity of 96%. The uranium was precipitated with NH_4OH, and the precipitate was calcined to the oxide at 900°C. The total oxide weight of product A15-2 was 11.034 g. Alpha pulse height data indicated 20.3 ppm of uranium-232 and 5.9 ppm of plutonium-238. Based on alpha pusle height data and proportional counting, the uranium-234 weight was calculated at 8.874 g. Mass analysis indicated product A15-2 had an isotopic purity of 96.225%.

In September 1977, final products 77-1 and A15-2 were shipped to Isotope Sales at ORNL along with final products A13-3B [46] and A15-1E [46] remaining from FY-1976 operations. Table 2 summarizes uranium-234 products shipped to meet FY-1977 production goal.

Separation research

Liquid thermal diffusion

W. M. Rutherford

Recent work on isotope separation by liquid phase thermal diffusion has been concerned with the effect of cooling water flow rate on the column coefficients. The large changes in separation that are observed appear to be directly related to the vertical temperature gradient imposed on the column by the finite water flow rate. The vertical temperature gradient is inversely related to the flow rate; hence, large temperature differences can be created by appropriate reduction of the flow rate.

Positive temperature gradients (temperature increasing upward) tend to suppress thermogravitational movement of fluid. It is believed that large-scale parasitic circulations caused by nonideal distribution of temperature in the horizontal direction are strongly inhibited by such gradients, whereas the normal thermogravitational circulation of the column is relatively unaffected. Thus, the separation is enhanced by reduction of the coolant flow rate.

As vertical temperature differences become large, they must be taken into account in calculating column coefficients from theory. The coefficients now become functions of vertical position, and in order to do the calculations, it is necessary to know the vertical distribution of temperature along the hot and cold walls. The hot and cold wall temperatures can be indirectly derived from the steam and cooling water temperatures

Table 2 - U-234 PRODUCTS SHIPPED (FY-1977)

Product	Oxide (g)	U-234 (g)	Isotopic Purity (%)	Pu-238 (ppm)
A13-3B	0.594	0.494	99.08	1.1
77-1	15.250	12.363	99.081	5.3
A15-1E	2.060	1.606	95.972	2.3
A15-2	11.034	8.874	96.225	5.9
Total	28.938	23.337		

by accounting for the several thermal resistances in the system.

Figure 10 is a schematic diagram of a typical column cross section from the steam tube through the water jacket. The thermal resistances in this configuration are as follows:

1) The falling film of steam condensate on the inner surface of the steam tube.
2) The metal comprising the hot wall or the column.
3) The working fluid in the annulus.
4) The metal comprising the cold wall of the column.
5) The convective heat transfer process from the outside of the cold wall to the coolant.

The local heat flow per unit-length, q, is given by

$$q = \frac{2\pi(T_S - T_w)}{\frac{2}{h_w D_4} + \frac{1}{S_{34}} + \frac{1}{S_{23}} + \frac{1}{S_{12}} + \frac{2}{h_S D_1}} , \quad (1)$$

where T_S = the steam temperature,
T_w = the bulk water temperature,
D_i = the diameter of the surface i (See Figure 10)
h_S = the heat transfer coefficient for condensing steam, and
h_w = the heat transfer coefficient to the coolant; and

$$S_{ij} = \frac{\bar{\lambda}_{ij}}{\ln Dj/Di} , \quad (2)$$

where $\bar{\lambda}_{ij}$, the average thermal conductivity in the region bounded by surfaces i and j, is given by

$$\bar{\lambda}_{ij} = \frac{\int_{T_i}^{T_j} \lambda(T)\, dT}{T_j - T_i} . \quad (3)$$

The temperatures of the several interfaces in the column are given by the following:

$$T_1 = T_s - q/\pi h_s D_1 \quad (4)$$

$$T_2 = T_1 - q/2\pi S_{12} \quad (5)$$

$$T_3 = T_2 - q/2\pi S_{23} \quad (6)$$

$$T_4 = T_3 - q/2\pi S_{34} \quad (7)$$

T_2 and T_3 are the hot and cold wall temperatures, respectively, in the working space.

According to Jacob [47], the transfer of heat from the inner tube of a cylindrical, vertical annulus to a fluid in laminar flow is described by the following empirical equation for the heat transfer coefficient:

$$h_w = 1.02\left(\frac{\lambda_a}{D_e}\right)\left(Re_a\right)^{.45}\left(Pr_a\right)^{.5}\left(\frac{\eta_a}{\eta_a}\right)^{.14}\left(\frac{D_e}{L}\right)^{.4}\left(\frac{D_5}{D_4}\right)^{.8} Gr^{.45} \quad (8)$$

where $D_e = D_5 - D_4$, (9)

η = viscosity, and
L = length of column,

The Prandtl, Reynolds and Grashof numbers are defined by:

$$Pr_a = C_{pa}\eta_a/\lambda_a \quad (10)$$

$$Re_a = 4W/\pi\eta_a(D_4 + D_5) \quad (11)$$

$$Gr_a = \rho_a^2 \beta_a (T_4 - T_5) D_e^3 g/\eta_a^2 \quad (12)$$

where C_p = heat capacity,
ρ = density
$\beta = -\frac{1}{\rho}\frac{d\rho}{dT}$, (13)
W = coolant flow rate,
g = acceleration of gravity,

and the subscript a denotes quantities evaluated at

$$T_a = (T_4 + T_w)/2 \quad (14)$$

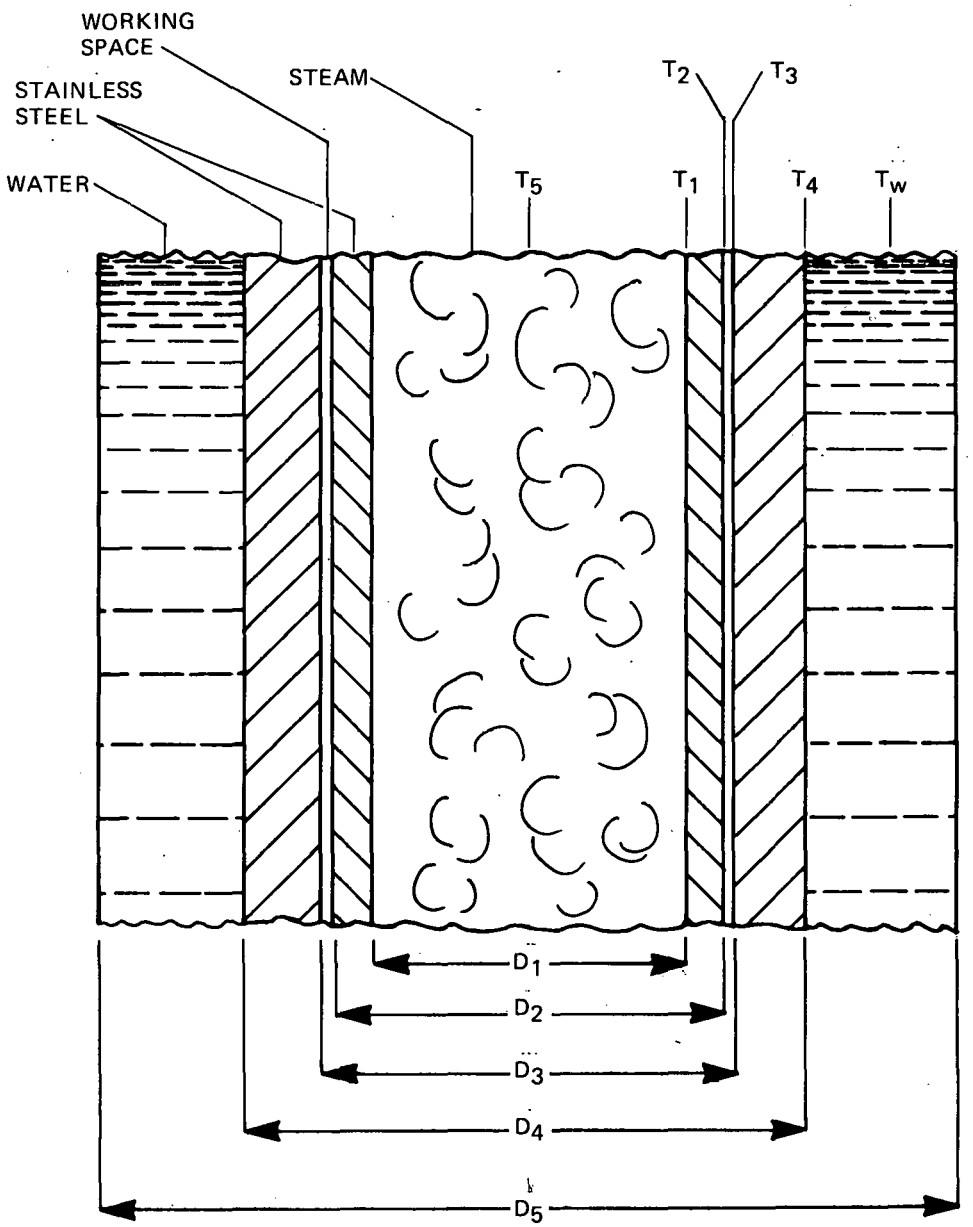

FIGURE 10 - Schematic cross section of liquid phase thermal diffusion column.

The problem of heat transfer through a falling film of steam condensate has been treated by Dukler [48]. According to Dukler, the heat transfer coefficient is given in terms of ξ, an empirical function of the Reynolds and Prandtl numbers of the condensate film and a quantity B which characterizes the effect of shear between the vapor and condensate phases. Thus,

$$h_S = \lambda_c \left(\frac{\rho_c^2 g}{\eta_c^2} \right)^{1/3} \xi \, (Re_c, Pr_c, B) \qquad (15)$$

where $Re_c = r\Gamma/\eta_c$, and (16)

Γ = local condensate flow per unit of perimeter.

The dimensionless interfacial shear parameter is given by the following empirical relationship:

$$B = \frac{\eta_c^{1.173}\eta_S^{0.16}\left(Re_{cL} - Re_c\right)^{1.4} Re_c^{0.4}}{4\, g^{2/3} D_l^{\,2} \rho_c^{0.553} \rho_S^{0.78}} \qquad (17)$$

In the above equations the subscripts have the following meanings:

c = condensate quantity,
S = steam quantity, and
L = quantity evaluated at z = L, thus at the bottom of the column.

The quantity ξ is presented in a series of graphs contained in a supplement to Reference 48. These cover the ranges $100 > Re > 80{,}000$, $0.1 > Pr > 10$, and $0 > B > 4{,}000$, including nearly all conditions of practical interest.

Equations 1 through 17 provide the means for evaluating the horizontal temperature distribution in the thermal diffusion column. The vertical temperature distribution can now be evaluated based on the following conditions:

1) The (saturated) steam temperature is constant as a function of position.
2) The coolant enters the water jacket at the bottom at a temperature T_{Wi} and exits at the top.
3) The steam condensate flow is zero at the top ($\Gamma = 0$ at $z = 0$).

There are two approaches to the problem. We can start at the top with a known condensate flow and an assumed water outlet temperature and integrate toward the bottom, iterating on the assumed outlet temperature until a match is obtained between calculated and specified water inlet temperatures. Conversely, we can start at the bottom with an assumed condensate flow and iterate on condensate flow until $\Gamma = 0$ at the top.

The first method was arbitrarily chosen. Thus, the local water temperature is given by

$$T_W = T_{WF} - \int_0^z (q/WC_p)\, dz \qquad (18)$$

and the local condensate flow by

$$\Gamma = \frac{1}{\pi D_l} \int_0^z (q/\Delta H_v)\, dz \qquad (19)$$

where ΔH_v is the enthalpy of vaporization of the steam.

A simple trapezoidal integration of Equations 18 and 19 is quite adequate. It should be noted, however, that the evaluation of q at each point involves an additional iterative calculation because h_W and the S_{ij} are temperature dependent.

A computer program was written to solve Equations 1 though 19. Temperature distributions and total heat flow were evaluated as functions of water flow rate for three experimental columns using chlorobenzene and carbon disulfide as working fluids. The interfacial shear parameter was assumed to be zero for these calculations; however, this should have a relatively minor effect on the results. Column dimensions and other data are given in Table 3.

The temperature rise of the cooling water and the total heat flow are plotted in Figures 11 and 12 for several cases.

Figure 13 depicts the hot and cold wall temperatures of one of the columns operating at a water flow rate thought to be close to optimum for this particular device. Although the bulk water temperature

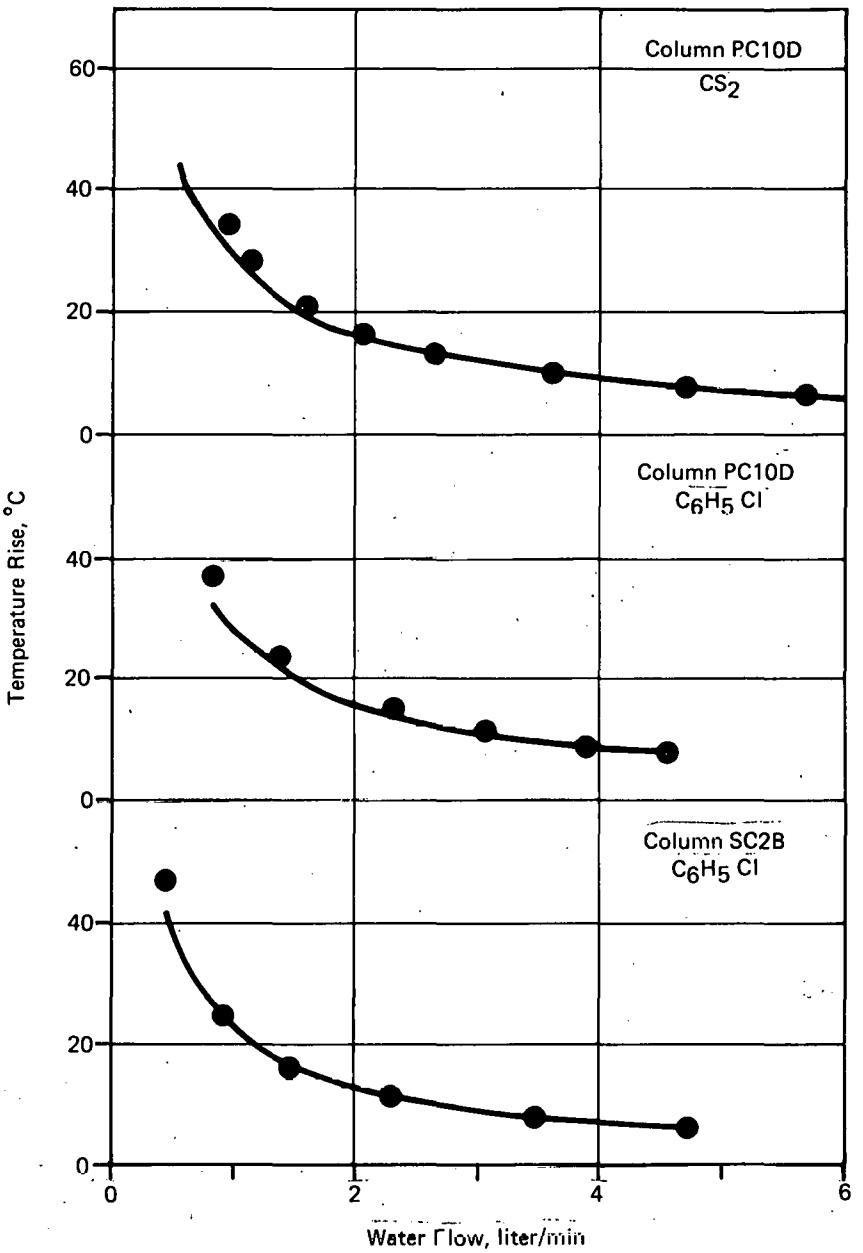

FIGURE 11 - Temperature rise of cooling water in experimental thermal diffusion columns.

increases by nearly 30°C from top to bottom, the temperature difference between the top and bottom of the cold wall is 15.5° and the working temperature difference (hot wall to cold wall) changes by only 9.6° along the column.

An existing set of computer programs was used to calculate column transport coefficients as functions of length and water flow. A typical set of results, obtained for separation of sulfur isotopes using CS_2, is shown in Figure 14. In this figure, experimental values of the initial transport coefficient, H, the remixing coefficient, K, and the equilibrium separation parameter, Y, are compared to selected theoretical values. The experimental value of H was derived from transient measurements

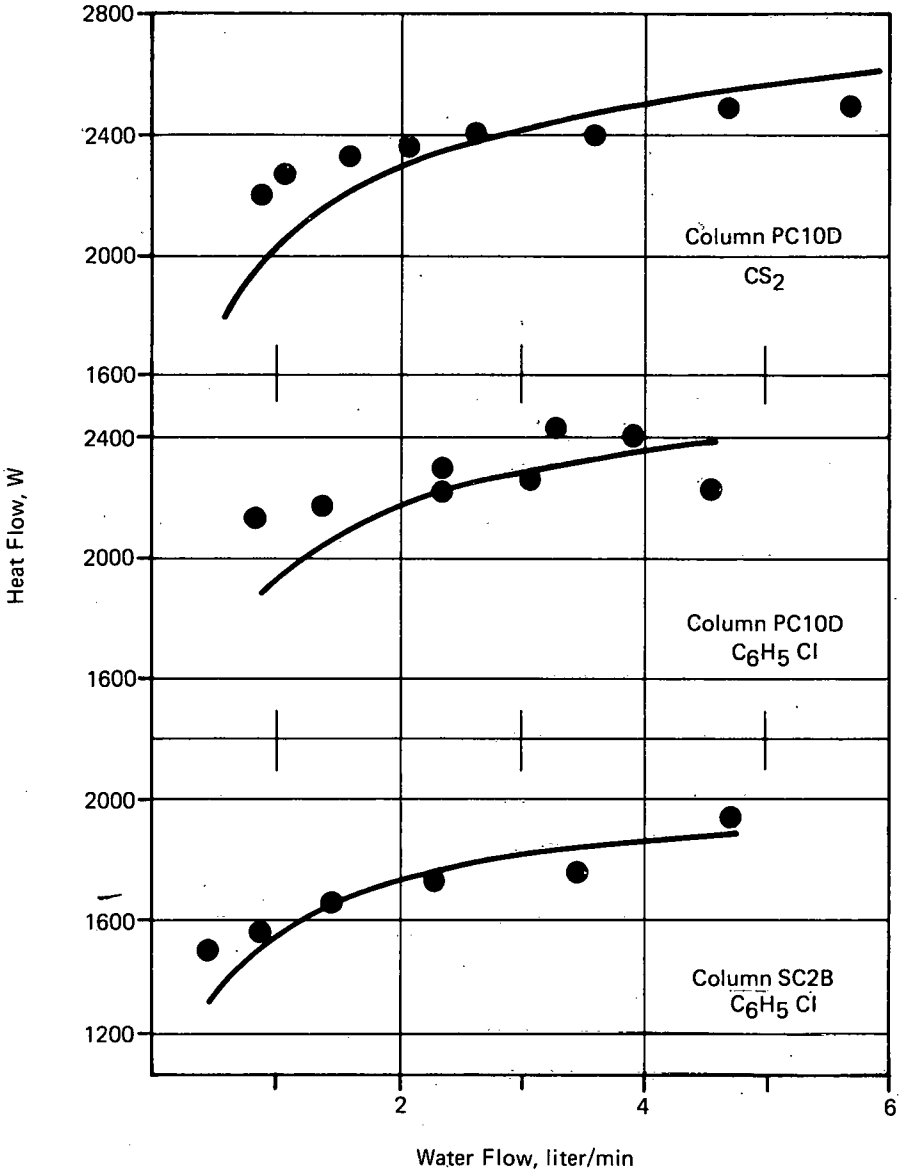

FIGURE 12 - Total heat flow as a function of cooling water flow in experimental diffusion columns.

using a large top reservoir; therefore, the theoretical value of H at z = 0 was selected as most appropriate for comparison. The theoretical quantities of K and Y were taken at the midpoint of the column, thus they represent average values.

The theoretical results shown in Figure 14 are based upon a value of 0.06 for the isotopic thermal diffusion factor of $C^{32}S_2 - C^{32}S^{34}S$. This number was obtained in early transport measurements [49] with a research column operated at a high water flow, hence, a small vertical temperature gradient.

Table 3 - DIMENSIONS AND OPERATING CONDITIONS FOR LIQUID PHASE THERMAL DIFFUSION COLUMNS[a]

Column	L	D_1	D_2	D_3	D_4	D_5	a (μm)[b]	T_s	T_{Wi}
SC2B	61	1.45	1.8771	1.9279	2.54	5.05	254	164	15
PC10D	61	1.93	2.5072	2.5580	3.81	6.26	254	164	15
SC5	76	1.61	1.9230	1.9637	2.54	5.05	203	164	15

[a]Dimensions in cm and temperatures in °C unless otherwise indicated.
[b]a is the spacing between the hot and cold walls.

Table 4 - PARAMETERS FOR LIQUID THERMAL DIFFUSION COLUMN SC5

Parameter	Theory	Expt.
10^5H (g/sec)	0.593	0.425
K (g-cm/sec)	0.000262	0.000193
Y	1.671	1.65
$T_{WF}-T_{Wi}$	39.2	33.8
Total Heat Flow	2121	2460

Table 4 contains data for a column with a much smaller hot-to-cold wall spacing of 200 μm. Chlorobenzene was used as the working fluid. At this spacing, the column time constant becomes rather large; therefore, data were obtained for only one water flow rate. The isotopic thermal diffusion factor for the $C_6H_5{}^{35}Cl$ -$C_6H_5{}^{37}Cl$ separation was taken to be 0.02 on the basis of earlier, unreported total reflux measurements in a 60-cm research column.

On the basis of these results, it appears that the thermal behavior of liquid thermal diffusion columns can be predicted with a resonable degree of accuracy. Discrepancies between calculated and observed total heat flow were less than 14% and in most cases less than 5%. Deviations were largest at the lowest flow rates, possibly as the result of end effects.

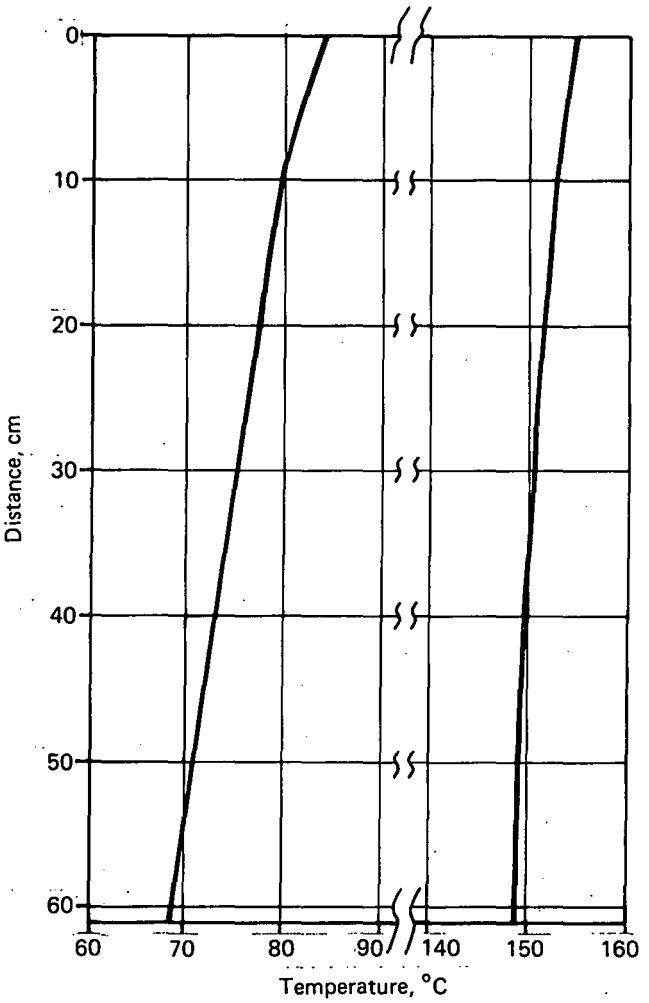

FIGURE 13 - Calculated hot and cold wall temperatures for column PC10D. CS_2 working fluid; water flow, 1.33 liter/min.

The measured column transport coefficients reported herein were obtained by a transient technique. The data are rather scattered and the agreement between theory

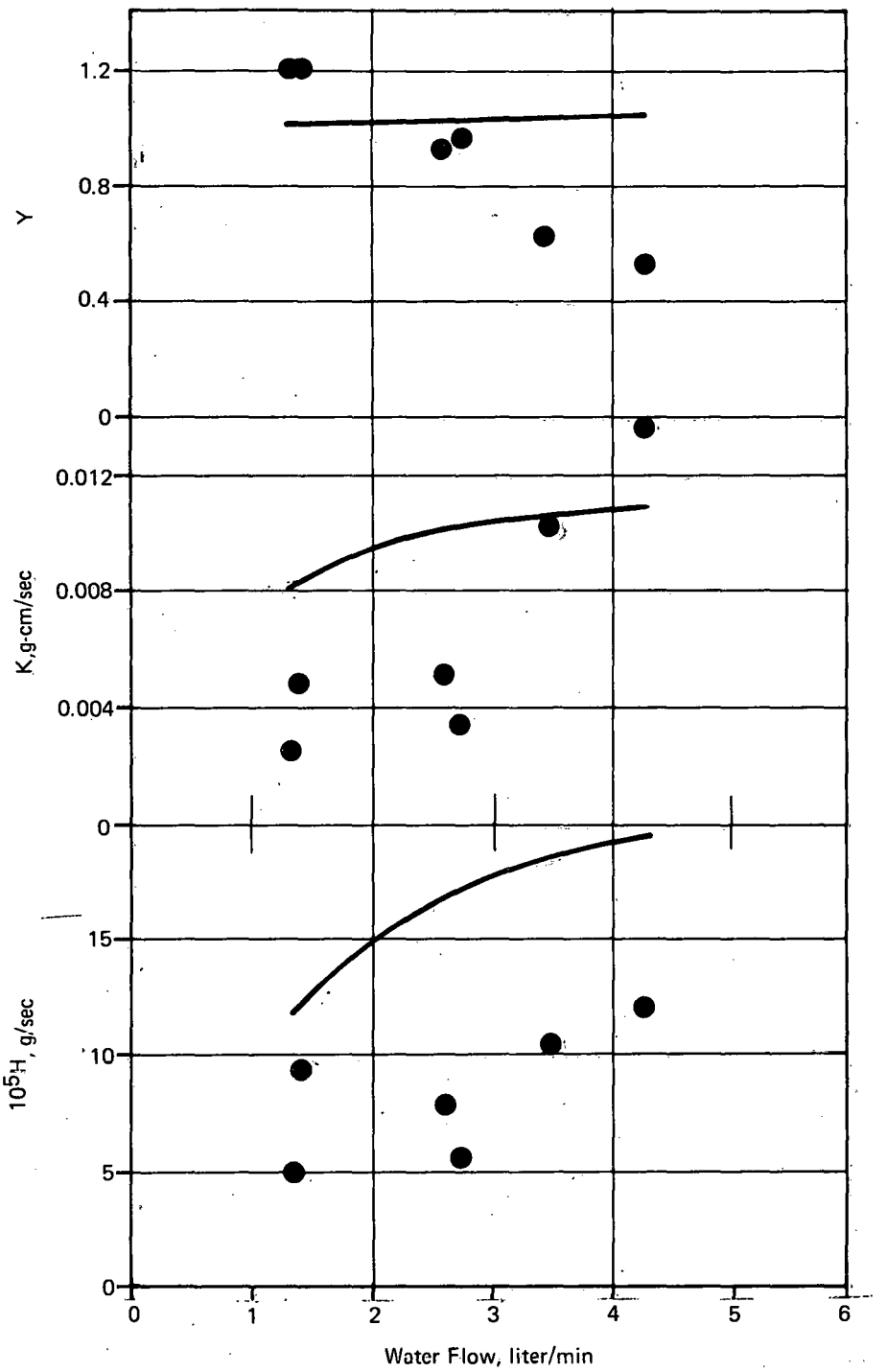

FIGURE 14 - Calculated and measured column coefficients for the $C^{32}S_2$ - $C^{32}S^{34}S$ separation in column PC10D.

and experiment is generally poor. The poor agreement may result from problems with the transient technique. Additional measurements in the future will be made by the steady state flow technique which is thought to be much more reliable.

Molecular beam scattering

R. W. York

The secondary beam source Cryotip refrigerator was returned to the manufacturer earlier this year for repair. The rebuilt Cryotip has since been received and tested satisfactorily. It was then once again installed on the beam source, and the alignment of the beam forming components was reset. This completed the secondary arm of the beam chamber, making it operational.

Velocity selector mounting hardware was designed and fabricated for a new high-speed drive motor. A stainless-steel, ported vacuum-chamber dome was built to house the selector test system on a bell-jar pumping station. Dynamic testing of the selector will be performed using an effusive beam source and ion gage detector to measure velocity distributions prior to installation in the molecular beam chamber.

The vacuum pumpdown in the detector section of the beam chamber leveled off at about 3×10^{-7} torr, a higher pressure than the maximum of 1×10^{-8} torr necessary for definitive crossed beam testing of the quadrupole detector system. Nevertheless, it was decided to investigate the capability of the detector for resolving crossed beam scattering intensities using an argon-argon scattering system prior to continuation of total scattering cross section measurements.

The detector tests were greatly hampered by noise and signal drift problems caused by the high pressure, complexity of the system, and the many potential sources of instability involved. One of the major problems was RF frequency drift which was continuously monitored during operation. In an attempt to remedy this problem, several crystals were purchased for fixed-frequency drive operation. Also, a vacuum leak was found at a major sealing surface in the titainium sublimation pump mounting. This leak was large enough to account for the 10^{-7} torr range limit. The titanium pump housing was removed from the chamber to have an O-ring groove machined in the mounting flange. This standard O-ring permitted better vacuum seal than did the special-order Gask-O-Seal previously used. The chamber is currently being evacuated in an attempt to reach the 10^{-8} torr range for a final crossed beam trial measurement. If it is unsucessful, total cross section experiments will resume with the new target cell and quadrupole detector system.

Transport properties

MUTUAL DIFFUSION OF KRYPTON-NOBLE GAS SYSTEMS

D. Cain and W. L. Taylor

Background Diffusion in gases is the phenomenon resulting in the physical transfer of a species of molecule through a medium due to spatial differences in its concentration. The mathematical description of diffusion relates a flux or flow of particles to a negative concentration gradient. The proportionality constant between this flux and the negative concentration gradient is defined as the diffusion coefficient.

Knowledge of the diffusion process is of practical interest because of its important role in a wide variety of physical and chemical processes. Theoretically, diffusion coefficients along with other transport

property data, virial coefficients, and beam scattering data provide much of the information available on intermolecular forces.

Several years ago Dr. Stanley Weissman and Gary A. DuBro of Mound developed a method and constructed an apparatus to measure the diffusion coefficients of gases. The heart of the system is a diffusion cell consisting of two identical chambers positioned one above the other and connected by a capillary. The heavier gas is introduced into the lower chamber, the lighter gas into the chamber above, and the gases are allowed to mix while the change in composition in each of the chambers is measured as a function of time. The major advantages of the method are (1) it involves no moving parts, and (2) it is independent of the initial conditions. With the present system it is possible to measure the diffusion coefficients of gases in a cryogenic environment or up to elevated temperatures limited only by the materials of construction of the diffusion cell. Several publications resulted from the previous work of Weissman and DuBro [50-57]. Unfortunately, the diffusion cell used in that previous work was ruined when the temperature was raised over 1400°K, and the flat end plates collapsed. A new cell has been constructed which will be described in detail in another section of this report. The purpose of the present work is to accurately measure the diffusion coefficent of krypton-noble gas systems over the temperature range 300 to 1200°K, using the new diffusion cell. The simplicity of the theory and the advantages of the experimental apparatus make this a precise and reliable method for such measurements.

Theory Consider two volumes, V_1 and V_2, connected by a tube of uniform cross-sectional area, A, and of length, L. Let each volume be filled with a gas of known composition, the compositions not being the same in V_1 as in V_2, but the pressures being equal. By virtue of the difference in composition of the gases in each volume, a concentration gradient will be established across the connecting tube, and gas will diffuse through the capillary until all concentration gradients have disappeared and the composition is uniform throughout both volumes and the tube.

In order to develop the theory describing the diffusion process outlined above, certain assumptions will be made and the necessary corrections made later. The assumptions are:

a) the concentration gradient in the connecting tube is linear,
b) the concentration gradients exist only in the connecting tube, and
c) the volume of the connecting tube is negligibly small compared to V_1 or V_2.

As previously stated, the coefficient of diffusion of gas species 1 through species 2 (here denoted as D_{12}) is defined as the proportionality constant between a particle flux and a negative concentration gradient. Mathematically this satement is expressed by Fick's first law of diffusion.

$$\Phi = -D_{12} \nabla\chi(t) \qquad (1)$$

where Φ is the particle flux in number of particles crossing a unit area in unit time, $\chi(t)$ is the concentration of the species at time t in (moles/cm^3), ∇ is the gradient operator, and D_{12} is the diffusion coefficient in cm^2/sec. Since, by assumption, the gradient exists only in the connecting tube and varies linearly along the direction of the tube (here taken

to be the z-direction), the following substitution for the concentration in the tube can be made

$$\nabla\chi(t) = \frac{d\chi(t)}{dz} = \frac{\chi_2(t) - \chi_1(t)}{L} \qquad (2)$$

and thus

$$\Phi = -D_{12} \frac{\chi_2(t) - \chi_1(t)}{L}. \qquad (3)$$

Here $\chi_2(t)$ and $\chi_1(t)$ are the concentrations of the gas component in volumes 2 and 1, repectively, at time t. The particles originate from one of the volumes, V_2, say, and diffuse through the area A of the tube. Thus

$$\Phi = \frac{1}{A}\frac{d}{dt}[V_2\chi_2(t)] = \frac{V_2}{A}\frac{d\chi_2(t)}{dt} \qquad (4)$$

where $V_2\chi_2(t)$ is the number of particles of the species of interest in volume V_2 at time t. Equating Equations 4 and 3

$$\frac{V_2}{A}\frac{d\chi_2(t)}{dt} = -D_{12}\frac{\chi_2(t) - \chi_1(t)}{L}. \qquad (5)$$

Neglecting the volume of the connecting tube (assumption c), conservation of mass gives

$$V_1\chi_1(t) + V_2\chi_2(t) = V_o\chi_\infty \qquad (6)$$

where $V_o = V_1 + V_2$ and χ_∞ is the concentration in both volumes after equilibrium has been reached ($t = \infty$). Solving Equation 6 for $\chi_1(t)$, substituting into Equation 5, and simplifying, one gets

$$\frac{d\chi_2(t)}{dt} = -D_{12}\frac{AV_o}{LV_1V_2}\chi_2(t) + D_{12}\frac{AV_o\chi_\infty}{LV_1V_2}$$

$$\frac{d\chi_2(t)}{dt} = -\gamma\chi_2(t) + \delta \qquad (7)$$

where $\gamma = D_{12}\frac{AV_o}{LV_1V_2}$ and $\delta = \frac{D_{12}AV_o\chi_\infty}{LV_1V_2}$. (8)

With γ and δ constants in time

$$\frac{d\chi_2(t)}{dt} = \frac{d}{dt}[\chi_2(t) - \delta/\gamma]$$

and Equation 7 can be written

$$\frac{d}{dt}[\chi_2(t) - \delta/\gamma] = -\gamma[\chi_2(t) - \delta/\gamma]$$

$$\frac{d}{dt}[\chi_2(t) - \chi_\infty] = -\gamma[\chi_2(t) - \chi_\infty] \qquad (9)$$

where the last step is $\delta/\gamma = \chi_\infty$ by Equations 8. Equation 9 can be integrated directly

$$\frac{d[\chi_2(t) - \chi_\infty]}{[\chi_2(t) - \chi_\infty]} = -\gamma\,dt$$

$$\int_o^t \frac{d[\chi_2(t') - \chi_\infty]}{[\chi_2(t') - \chi_\infty]} = \int_o^t -\gamma\,dt'$$

$$\ln\left[\frac{\chi_2(t) - \chi_\infty}{\chi_2(o) - \chi_\infty}\right] = -\gamma t \qquad (10a)$$

$$\chi_2(t) - \chi_\infty = (\chi_2(o) - \chi_\infty)\,e^{-\gamma t} \qquad (10b)$$

The above solution to the diffusion equation is from Ney and Armistead [58] who were the first experimenters to use the two-bulb gaseous diffusion apparatus. This relation can be put into a more convenient form by writing an equation similar to (10b) for the composition of the gas component in volume 1 and subtracting from (10b)

$$\chi_1(t) - \chi_\infty = [\chi_1(o) - \chi_\infty]e^{-\gamma t} \qquad (10c)$$

$$\chi_2(t) - \chi_1(t) = [\chi_2(o) - \chi_1(o)]e^{-\gamma t} \qquad (11)$$

Making the substitutions

$$\chi_2(t) - \chi_1(t) = \Delta\chi(t)$$

$$\chi_2(o) - \chi_1(o) = \Delta\chi(o)$$

one arrives at the following compact form

$$\Delta\chi(t) = \Delta\chi(o)e^{-\gamma t} \qquad (12)$$

where γ represents the reciprocal of the relaxation time of the diffusion process.

Equation 12 is the solution to the diffusion Equation 1 for the given assumptions. It is now necessary to modify this relation to account for deviations from this idealization.

Assumption a (linear concentration gradient) led to Equation 2 for the concentration gradient; this implies that $\nabla^2\chi(t) = \partial^2\chi(t)/\partial z^2 = 0$. This result coupled with the diffusion equation in partial differential form [59], $\partial^2\chi(t)/\partial z^2 = D_{12}\partial^2\chi/\partial t^2$ (which is just Fick's second law of diffusion [60]) reveals that this first assumption is that the diffusion takes place in the steady-state ($\partial\chi/\partial t = 0$). This is actually true only for capillary connecting tubes and infinite volumes, though it is approximately true for volumes that are large compared to that of the capillary.

R. Paul has discussed the assumption of the steady-state in some detail [61]. The flow through the diffusion tube is actually non-uniform, resulting in a reduction of flux through the tube and an accumulation of gas in the tube. This effectively increases the relaxation time γ^{-1} which appears in Equation 12. The proper form of the inverse relaxation time as worked out by Paul is

$$\gamma' = \gamma\left(1 - \frac{\gamma V_1^2 L^2}{D_{12}V_o^2}\right)^{1/2} \approx \gamma\left(1 - \frac{AL}{2V_o}\frac{V_1}{V_2}\right) \qquad (13)$$

In considering the second assumption, one can solve Equation 12 for the diffusion coefficient D_{12} in terms of concentrations and geometric factors, leading to a direct proportionality between D_{12} and L/A of the connecting tube. Since the volumes connected by the tube are not infinite, they also have an L_v/A_v in which a concentration gradient can exist. Therefore, the L/A to which D_{12} is proportional must be interpreted as $\sum_i L_i/A_i$ where the sum extends over each volume and the capillary. However, the L_v/A_v for the apparatus used is negligibly small when compared to that of the connecting tube ($\leq$0.2%). Thus the assumption that the concentration gradient is confined to the connecting tube is justified provided that a small end correction is made.

The end correction is mathematically and physically similar to those considered by Maxwell [62] for electric current flow and by Rayleigh [63] for sound passage in a tube. The form of the correction is

$$L_{eff} = L + 2\,\alpha r \qquad (14)$$

where L_{eff} is the effective length of the connecting tube, L is its actual length, r is its radius, and α is a numerical constant which depends on the geometric configuration of the apparatus. The factor 2 accounts for the two ends of the tube. An α value of 0.58 is proper for this apparatus. This correction increases the effective length of the connecting tube to account for the fact that the concentration gradient does not truncate at the ends of the tube.

In treating the negligibility of the connecting tube volume (assumption c), a second approximation will be used. It may be assumed that the average concentration in the connecting tube at any time is the average value of the concentration at the ends of the tube. Thus

$$\chi_L(t) = \frac{1}{2}\left[\chi_2(t) + \chi_1(t)\right]$$

and conservation of mass gives

$$(V_o + AL)\chi_\infty = V_2\chi_2(t) + V_1\chi_1(t) + \chi_L\, AL$$

$$(V_o + AL)\chi_\infty = (V_2+AL/2)\chi_2(t) + (V_1+AL/2)\chi_1(t).$$

This result can be incorporated into the theory by replacing V_o by V_o+AL, V_1 by $V_1+AL/2$, and V_2 by $V_2+AL/2$ in Equation 8 for γ.

$$\gamma = D_{12}\frac{A}{L}\frac{V_o+AL}{(V_1+AL/2)(V_2+AL/2)}. \qquad (15)$$

Using Equations 12, 13, 14, and 15 one arrives at the following results:

$$\Delta\chi(t) = \Delta\chi(o)e^{-\gamma' t} \qquad (16)$$

$$\gamma' = D_{12}\frac{A}{L_{eff}}\frac{V_o + AL}{(V_1+AL/2)(V_2+AL/2)}\left(1-\frac{AL}{2V_o}\frac{V_1}{V_2}\right)$$

$$\gamma' = D_{12}\, f(G) \qquad (17)$$

Here f(G) is an obvious function of the geometry of the apparatus

$$f(G) = \frac{A}{L_{eff}}\frac{V_o + AL}{(V_1+AL/2)(V_2+AL/2)}\left(1-\frac{AL}{2V_o}\frac{V_1}{V_2}\right). \qquad (18)$$

Taking the natural logarithm of Equation 16 yields

$$\ln\Delta\chi(t) = -\gamma' t + \ln\Delta\chi(o)$$

$$\ln\Delta\chi(t) = -D_{12}\, f(G)t + \ln\Delta\chi(o) \qquad (19)$$

This is a linear function between $\ln\Delta\chi(t)$ and t, the slope of which is directly proportional to D_{12}.

According to the Chapman-Enskog relation for the first approximation to the theoretical diffusion coefficient for a dilute gas [64], the diffusion coefficient is inversely proportional to the pressure, p, at which the process takes place. Thus the product pD_{12} is constant and values of D_{12} can be normalized to atmospheric pressure (denoted D°_{12}) by the relations

$$p_{atm}D^\circ_{12} = pD_{12} \qquad (20)$$

$$D^\circ_{12} = pD_{12}/p_{atm}. \qquad (21)$$

Equation 20 expresses the equality of the product pD_{12} at atmospheric pressure (p_{atm}) and at the pressure p at which the experiment is conducted. Equation 21 is the relation for the normalized diffusion coefficient in terms of the value obtained at the pressure p. Equation 21 can be used in Equations 17 and 19 to give

$$\gamma' = \frac{p_{atm}}{p}D^\circ_{12}\, f(G) \qquad (22)$$

$$\ln\Delta\chi(t) = -D^\circ_{12}\, p_{atm}\, f(G)t/p + \ln\Delta\chi(o)$$

$$\ln\left[\frac{\Delta\chi(t)}{\Delta\chi(o)}\right] = -D^\circ_{12}\, p_{atm}\, f(G)t/p. \qquad (23)$$

These equations allow for comparison of values of the diffusion coefficients of a particular system measured in different experiments at different pressures.

Equations 22 and 23 also suggest an experimental procedure which might be followed. The volumes V_1 and V_2 can be filled with gases of known (different) compositions at a known pressure p. At time t=0 they are allowed to begin mixing; at time t the experiment is halted and the gases in V_1 and V_2 are analyzed for composition. From the initial and final concentration differences and the values of t, p, and f(G) for the experiment, D°_{12} can be calculated. Alternately, several experiments on the same system can be run. Each experiment would yield a point on a plot of $\left(\ln\left[\frac{\Delta\chi(t)}{\Delta\chi(o)}\right]\right.$ as a function of t/p).

All the points should fall on a straight line through the origin, the slope of that line leading to D°_{12} for the system of study.

The procedures described above have been used by several experimenters in the past [65,72,76]. Such procedures have, however, the disadvantage of yielding only one determination of D°_{12} per experiment (necessitating an averaging process over all experiments) or only yielding one point per experiment on a straight line (requiring a least squares fit over all experimental points).

In the method used in the present study, each experiment can be considered as a series of experiments performed one after the other. The initial conditions for one experiment are the terminal conditions of the previous one, and each part is conducted at a slightly lower pressure than the part before. This is accomplished by withdrawing several small samples of gas for concentration analysis at intervals during the experiment. The removal of gas causes the reduction in pressure and requires some additional alterations to Equations 22 and 23.

For an experiment begun at $t = 0$, $p = p_1$, and sampled at $t = t_1$, Equation 22 can be written

$$\ln \Delta\chi(t_1) = -D^{\circ}_{12} \frac{p_{atm}}{p_1} f(G) t_1 + \ln \Delta\chi(o). \quad (24)$$

As a result of the sampling, the pressure is reduced to p_2, and the experiment is allowed to run until $t=t_2$. At this time another sample is drawn, and this part of the experiment has run at pressure p_2 for a length of time t_2-t_1:

$$\ln \Delta\chi(t_2) = -D^{\circ}_{12} \frac{p_{atm}}{p_2} f(G) \ (t_2-t_1) + \ln \Delta\chi(t_1). \quad (25)$$

The experiment continues at the new pressure, p_3, until time t_3, having run for a length of time t_3-t_2 and

$$\ln \Delta\chi(t_3) = -D^{\circ}_{12} \frac{p_{atm}}{p_3} f(G) \ (t_3-t_2) + \ln \Delta\chi(t_2). \quad (26)$$

The nth sample drawn leads to the equation

$$\ln \Delta\chi(t_n) = -D^{\circ}_{12} \frac{p_{atm}}{p_n} f(G) \ (t_n-t_{n-1}) + \ln \Delta\chi(t_{n-1}) \quad (27)$$

Equations 24, 25, 26, and 27 represent a family of straight lines $\ln \Delta\chi(t_i)$ vs. $(t_i-t_{i-1})/P_i$, $i = 1, 2, 3, \ldots, n$. The slopes of these lines are all equal, but their intercepts are all different. Any one of them can be used to determine D°_{12}.

The above-mentioned equations can be made to describe one line. This is realized by substituting Equation 24 into 25 for $\ln \Delta\chi(t_1)$ to give $\ln \Delta\chi(t_2) = -D^{\circ}_{12} \ p_{atm} \ f(G) \times \left[\frac{t_2-t_1}{p_2} + \frac{t_1}{p_1}\right] + \ln \Delta\chi(o)$.

Rearranging,

$$\ln \Delta\chi(t_2) = -D^{\circ}_{12} \ p_{atm} \ f(G) \left[\frac{t_2}{p_2} + t_1\left(\frac{p_2-p_1}{p_1p_2}\right)\right] + \ln \Delta\chi(o). \quad (28)$$

Similarly Equation 28 can be used to eliminate $\ln \Delta\chi(t_2)$ in Equation 26:

$$\ln \Delta\chi(t_3) = D^{\circ}_{12} \ p_{atm} \ f(G) \left[\frac{t_2}{p_3} + t_2\left(\frac{p_2-p_1}{p_2p_3}\right) + t_1\left(\frac{p_2-p_1}{p_1p_2}\right)\right] + \ln \Delta\chi(o). \quad (29)$$

The nth equation is

$$\ln \Delta\chi(t_n) = -D^{\circ}_{12} \ p_{atm} \ f(G) \left[\frac{t_n}{p_n} + \sum_{i=1}^{n} t_{i-1} \times \left(\frac{p_i-p_{i-1}}{p_ip_{i-1}}\right)\right] + \ln \Delta\chi(o). \quad (30)$$

The expression in brackets has units of time/pressure and may be replaced by a single variable

$$\beta_n = \frac{t_n}{p_n} + \sum_{i=1}^{n} t_{i-1} \left(\frac{p_i - p_{i-1}}{p_i p_{i-1}} \right)$$

with $t_o = 0$. Equation 30 then reduces to

$$\ln \Delta\chi(t_n) = -D_{12}^{\circ} p_{atm} f(G) \beta_n + \ln \Delta\chi(o) \quad (31)$$

which is completely analogous to Equation 22. Thus each experiment provides n points on a plot rather than one point. Other experimenters have assumed that effects due to multiple sampling are negligible [66,67]; this development, however, accounts for the sampling and is due to Weissman and DuBro[51].

It can be seen from Equation 31 that the initial concentration difference $\Delta\chi(o)$ gives the intercept of the straight line. In the multiple sampling method, however, it is not necessary to know this quantity since each experiment yields several points through which a straight line may be fit. In the single method it is necessary to know this value, for it is used either in Equation 22 to determine a line through two points or in Equation 23 to normalize the values of the ordinate so that the plot will pass through the origin. Thus, by taking multiple samples, any time may be chosen as t=0 and the diffusion coefficient can be determined absolutely from the remaining data taken at t>0 and the $\ln \Delta\chi(t_i)$ vs. β_i plot.

Apparatus The primary component of the experimental apparatus is the diffusion cell. In addition to this, supportive systems are required for the purposes of evacuation, gas loading, environmental control and monitoring, and gas analysis.

The diffusion cell is shown before and after assembly in Figures 15a and 15b, respectively. A schematic of the diffusion cell plus support systems is given in Figure 16.

As can be seen in Figure 15a, the diffusion cell consists of two cylindrical chambers with hemispherical ends. The circular centerplate has the connecting tube welded through its center, perpendicular to the plane of the plate. One cell half is welded to each side of the center plate. Stainless-steel plugs were machined and welded in the hemispherical ends, and then the capillary feed lines were welded into the plugs.

The diffusion chambers, center plate, and connecting tube were constructed entirely of a nickel-base alloy, Hastelloy X (manufactured by Union Carbide). Each cell half was deep drawn from a flat sheet in a process known as hydroforming. This greatly reduced the amount of welding needed in construction, thereby eliminating possible leaks. As mentioned, the fittings for the feed lines were made of stainless steel, the feed lines themselves were 1/8 in. o.d. inconel. Pertinent cell dimensions are:

$V_1 = 1120.1 \text{ cm}^3$
$V_2 = 1121.1 \text{ cm}^3$
$L = 10.078 \text{ cm}$
$r = 0.1831 \text{ cm}.$

The diffusion cell was interconnected to the evacuation, loading, and sampling systems with copper tubing. Vacuum was achieved and maintained with a mechanical pump (Welch "Duo-seal" Model 1402) and a diffusion pump (Veeco, type EP2A, air cooled).

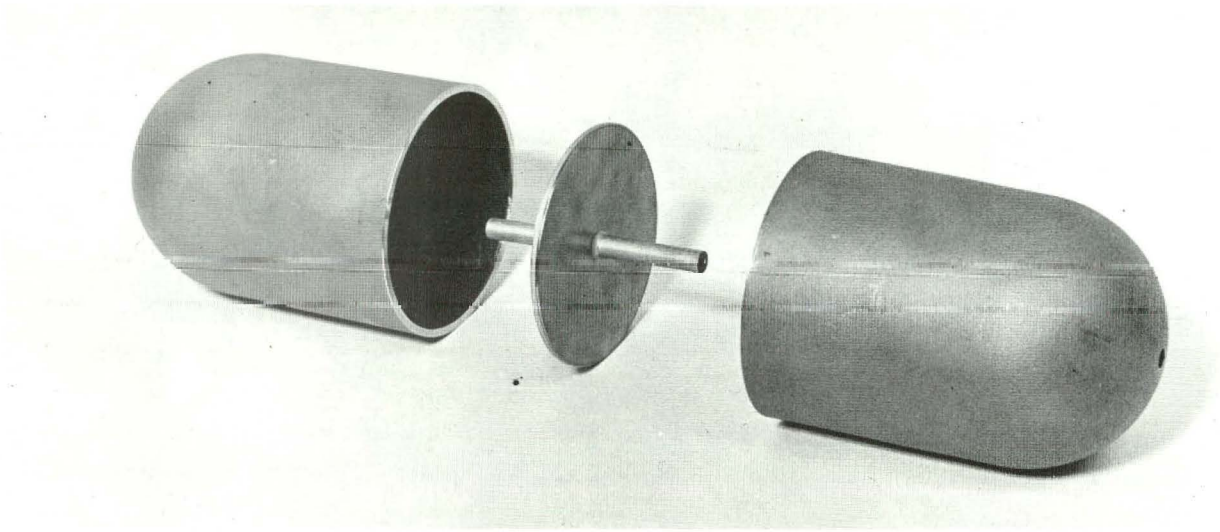

(a)

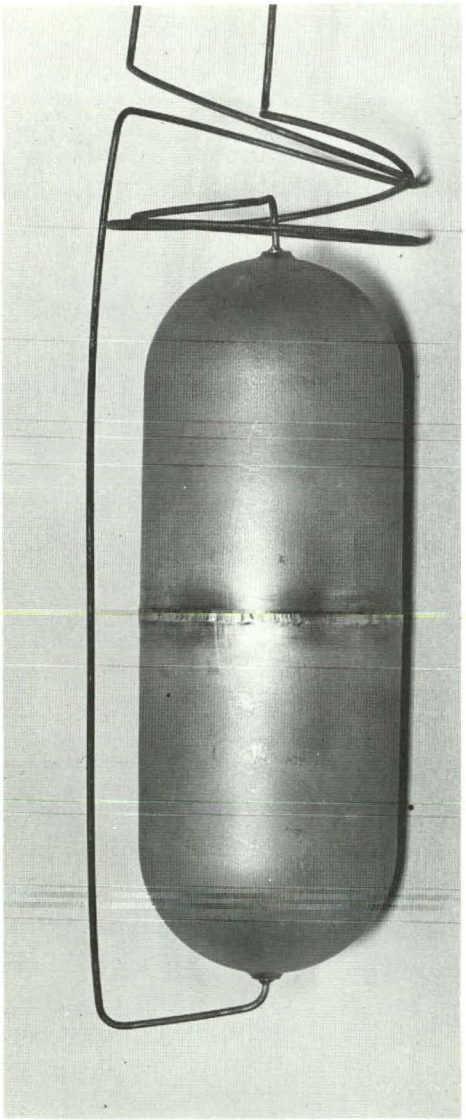

(b)

FIGURE 15 - Diffusion cell (a) before assembly showing the two chambers, center plate, and connecting tube, (b) after assembly with feed gas capillary lines attached.

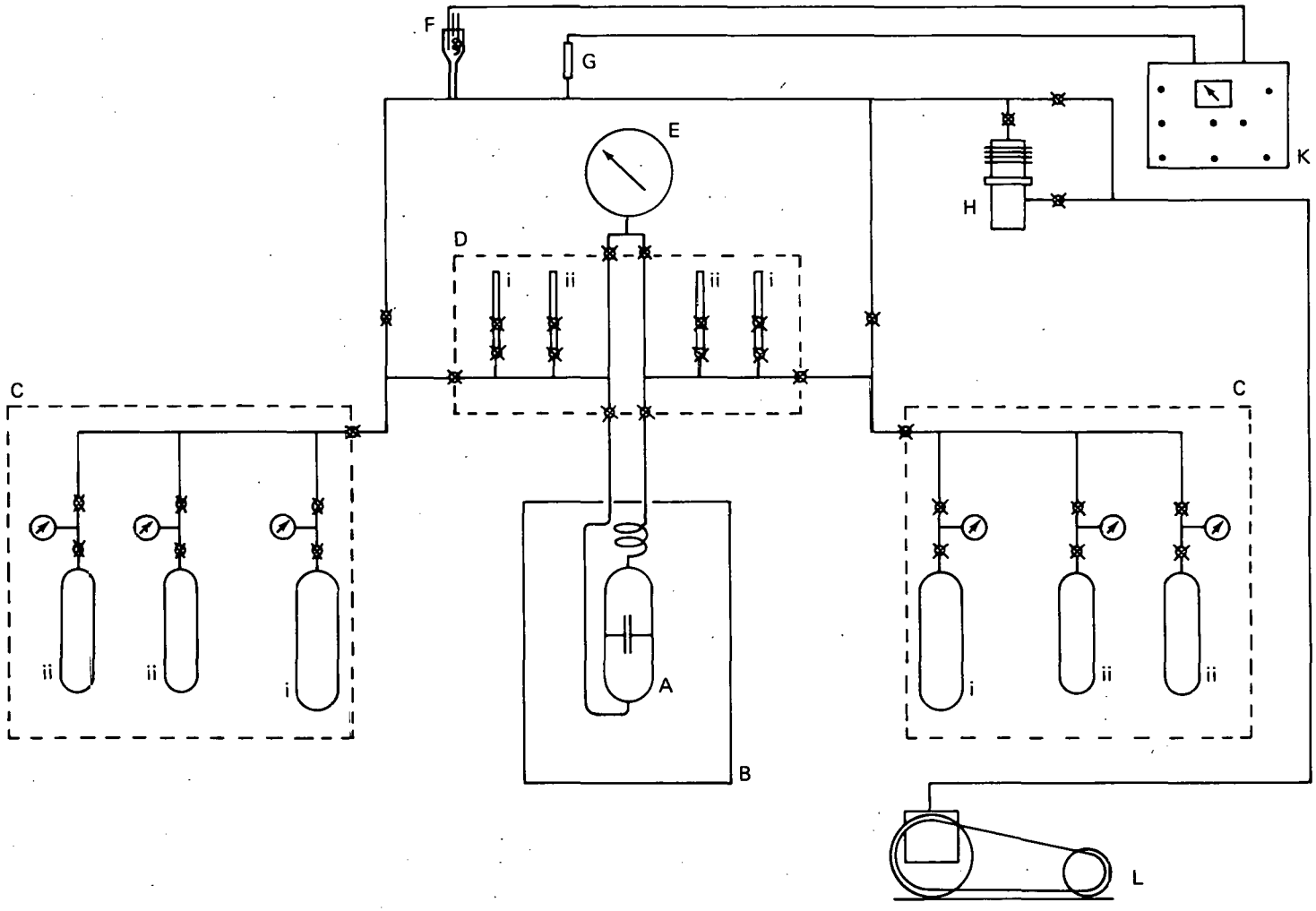

FIGURE 16 - Experimental apparatus showing A) diffusion cell; B) furnace; C) gas loading system with (i) feed gas storage tank and (ii) ballast tank; D) gas sampling system with (i) purge sample bottle and sample port, (ii) mass spectrometer sample bottle and sample port; E) Wallace and Tiernan pressure gauge; F) ionization gauge; G) thermocouple gauge; H) diffusion pump; K) NRC control console; L) mechanical pump.

The gas loading system consisted of a storage cylinder of the feed mixture for each of the diffusion chambers and two 0.5-liter cylinders for each chamber which served as ballast tanks. Samples were expanded into sample bottles which connected to the associated sampling capillaries by standard brass taper joints.

Environmental control was achieved by placing the diffusion cell in a three-zone tube furnace (Lindberg Hevi-Duty, Model 54756-A). Individual temperature regulation was possible in each of the three zones of the furnace. Temperatures were monitored both by a chromel-alumel thermocouple attached to the furnace controls and by a chromel-alumel thermocouple attached to the diffusion cell. Good thermal contact was maintained between the cell and the latter thermocouple by spot-welding strips of stainless steel shim stock over the thermocouple, holding it in physical contact with the cell over the length of half the cell. The tip of the thermocouple was shielded from direct radiation with asbestos, ensuring that the temperature indicated was that of the cell. Voltage readings on this latter thermocouple were balanced by a Honeywell potentiometer. Vacuum was measured with an NRC thermocouple gauage (NRC Model 501), an NRC ionization gauge (NRC Model 507), and an NRC thermocouple ionization gauge control console (NRC Model 710B). The gas pressures in the diffusion cell and the feed systems were observed on a Wallace and Tiernan precision dial manometer (Model FA-145) with a pressure range of 0 to 1050 torr. Gas analyses were performed on a modified C.E.C., Model 620 mass spectrometer.

Experimental Procedure The designs of the feed and sampling systems, as well as the procedure followed during experiments, were dictated by the design of the diffusion cell. In particular, the cell was built without moving parts, e.g., without a stopcock of any kind between the cell chambers.

The absence of a stopcock meant that gas mixtures had to be expanded separately and simultaneously from ballast tanks, through the connecting tubing, and into each cell chamber using PVT calculations to achieve the desired experimental conditions. Initial mixing of the gases inevitably takes place and turbulent, non-steady conditions exist during the loading. However, instabilities have been shown to die out rather quickly ($\sim$60-90 sec). Also, as noted above, the time t=0 is arbitrary and initial mixing does not affect the measurements. Therefore, the beginning time of the experiment can be chosen to be after a steady state is reached.

Gas sampling also had to be performed simultaneously and symmetrically with respect to the cell halves. The volumes of the diffusion chambers were made large and those of the sampling system small, so as to minimize disturbances due to abrupt changes in pressure during sampling.

Figure 16 clearly exhibits the symmetry of the support systems with respect to the diffusion cell. Pains were also taken to equalize volumes of the feed and sampling lines leading to each cell-half. The importance of this symmetry of design and procedure may perhaps be illustrated by the results of Mathur [67]. Though his loading technique met the criteria of the present study, his sampling technique did not. Mathur drew his samples from only one chamber of his diffusion cell, creating a pressure drop

across the connecting tube. His results show a large amount of scatter for the He-Ar system.

The initial step of an experiment is the evacuation of the entire system, except the gas storage tanks. During this time the furnace controls are set to the desired temperature and switched on. When the system pressure falls below 10^{-4} torr and the diffusion cell and furnace have reached thermal equilibrium, the feed gases can be loaded.

One side of the loading system, including its sample lines and the Wallace and Tiernan gauge, is isolated from the diffusion cell, the evacuation system, and the other loading system. The ballast tanks and feed lines are then filled with one gas up to the pressure needed to expand into the cell chamber at the final pressure and temperature being studied. The storage tank is closed off, the loading system is isolated, and the sampling system and pressure gauge are re-evacuated. This process is then repeated for the second gas on the other side.

The feed gases trapped in their respective feed systems and ballast tanks are now ready to be expanded simultaneously through their respective sampling systems and into the diffusion cell. This is done while isolated from the evacuation system and the Wallace and Tiernan gauge. Owing to the design of the system and the precautions taken, equal amounts of gas at equal pressures should enter into the equally sized chambers.

After 3 to 5 min have elapsed, the feed gases are simultaneously closed off from the diffusion cell, and the actual pressure of the gases in the cell is measured on the Wallace and Tiernan gauge. Another 60 to 90 sec is allowed for transient effects to die out, the diffusion cell is isolated, and the time is recorded. This is time t=0 for the experiment and all later times are measured relative to this. Again, any mixing which has already occurred will not affect the measurements, and the initial conditions at t=0 need not be known.

After the experiment commences two sample bottles are fitted into the sample ports on each side of the system. The sample lines and the associated sample bottles are pumped out. Two of the sample bottles are closed off (one on each side), while the other two are left open, but with the sample tubing closed off. At time $t=t_1$, both sides of the diffusion cell are opened to the sampling lines causing gas to expand into the evacuated volumes. After approximately 15 sec have elapsed, the bottles are closed, and the other two are opened. Gas is allowed to expand into these bottles for another 15 sec, and then they are closed off. The new cell pressure is measured and the diffusion cell is again isolated.

The first sample which is drawn from each cell half is discarded. This gas is withdrawn to purge the capillary feed tubes of material which may not reflect the composition of that in the larger chambers. The second samples are withdrawn and set aside for analysis. Additional sample bottles are installed in the sample ports and evacuated in preparation for the next sample withdrawal at $t=t_2$.

The above procedure of evacuation, purging, and sampling is followed five to nine times during the experiment. The number

of samples taken and the elapsed time between are governed by the duration and pressure of the experiment. The composition of each sample in the set is then determined by analysis on a Consolidated Electrodynamic Corporation (CEC) mass spectrometer. These results along with time and pressure data are used to determine the diffusion coefficent at the chosen temperature.

Experimental Results Equation 31 is the key relation for these diffusion measurements using the double chamber apparatus described above. The actual expression used in the data analysis is obtained by multiplying both sides of Equation 31 by -1:

$$-\ln \Delta\chi(t_n) = D^{\circ}_{12}\, p_{atm} f(G)\, \beta_n - \ln \Delta\chi(o). \quad (32)$$

As noted previously, the value of $\ln \Delta\chi(o)$ does not affect the results, and will be dropped from further consideration.

After the compositions of the samples are determined, a graph is plotted of $-\ln \Delta\chi(t_n)$ as a function of β_n. A straight line is then fitted to the data using the least squares method. The slope of this line, $D^{\circ}_{12}\, p_{atm}\, f(G)$ is set equal to γ' as in Equation 22 and solved for D°_{12}.

Figures 17 and 18 show data for two of the experiments, along with the least squares linear fit. These examples illustrate explicitly that the multiple sampling technique is consistent with the theoretical exponential approach to equilibrium provided the individual points are corrected for the pressure drop due to sample withdrawal.

Of the Krypton-noble gas combinations, krypton-xenon and krypton-argon have thus

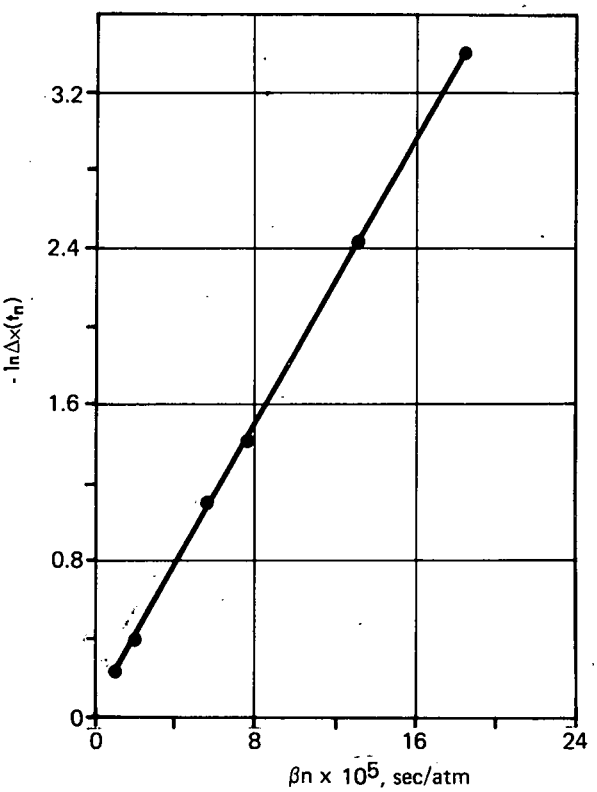

FIGURE 17 - Least squares linear fit of $-\ln \Delta\chi(t_n)$ as a function of β_n for Kr-Xe at 333.5°K.

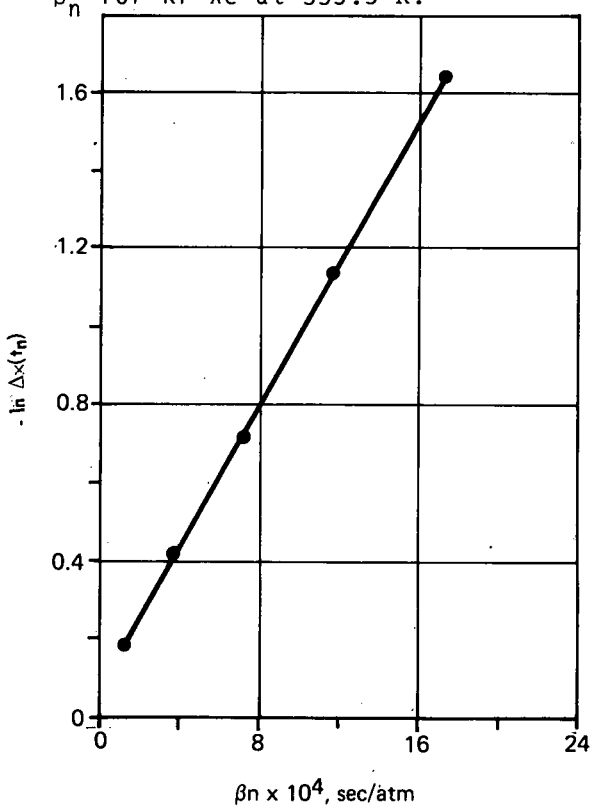

FIGURE 18 - Least squares linear fit of $-\ln \Delta\chi(t_n)$ as a function of β_n for Kr-Ar at 599.8°K.

far been investigated. Figure 19 shows the newly measured diffusion coefficients for krypton-xenon with the measurements (absolute) of other workers in a plot of $\log_{10} D^{\circ}_{12}$ as a function of $\log_{10} T$. As can be seen, the present measurements extend by over 400°K the temperature range over which diffusion coefficients have been determined. In the temperature region of overlap, the data fit within the scatter of values of other experiments. Table 5 lists the results of this study.

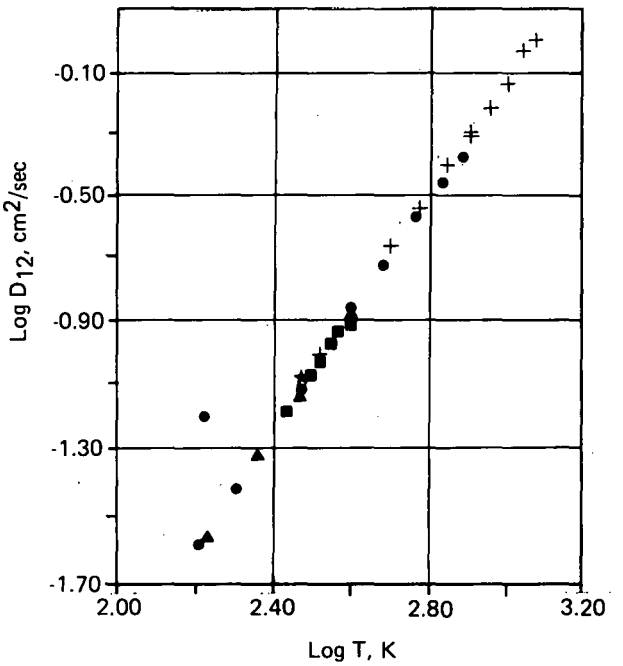

FIGURE 19 - Diffusion coefficient, D_{12}, as a function of temperature for Kr-Xe. The experimental points are: +, present work; ★, Watts (ref. 69); ■, Malinauskas (ref. 65); ●, Loiko, et al. (ref. 72); ▲, vanHeijningen, et al (ref. 70).

Table 5 - DIFFUSION COEFFICIENT MEASUREMENTS CORRECTED TO 1 ATMOSPHERE PRESSURE FOR Kr-Xe

Temperature (°K)	D_{12} (cm^2/sec)
333.5	0.099
394.0	0.136
505.8	0.223
599.7	0.295
715.3	0.401
813.1	0.506
814.0	0.517
911.6	0.621
1010.2	0.752
1112.5	0.960
1198.8	1.05

Figure 20 is a $\log_{10} D^{\circ}_{12}$ as a function of $\log_{10} T$ plot of the present results for krypton-argon and those of all other absolute measurements reported in the literature. Again the data are clustered together with the values of other investigations in those regions where temperatures overlap. Although the study of this system is not yet completed, it still represents an extension in temperature of more than 200°K for diffusion measurements with a dual chamber apparatus. The only other measurements as high, or higher, than the present ones were by Hogervorst [73], who used cataphoretic segregation of gas mixtures in a d.c. discharge tube

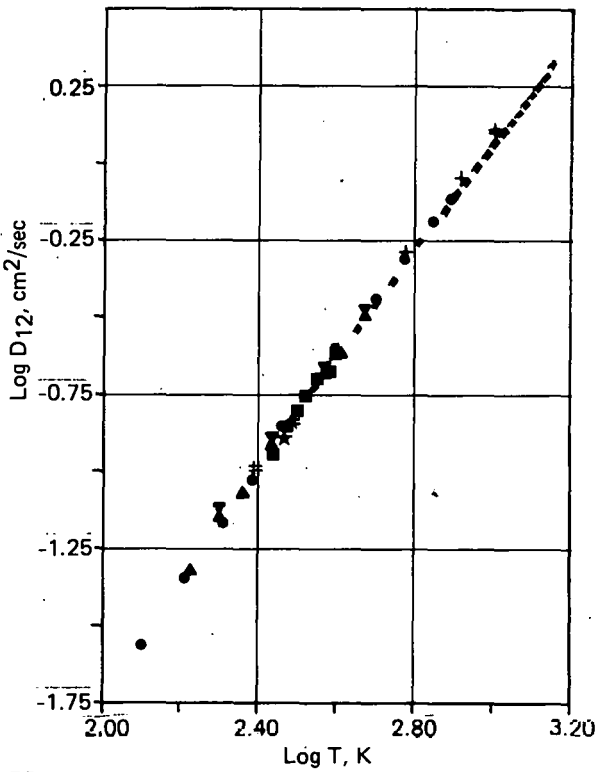

FIGURE 20 - Diffusion coefficient, D_{12}, as a function of temperature for Kr-Ar. The experimental points are: +, present work; ★, Watts (ref. 69); ■, Malinauskas (ref. 65); ●, Loiko, et al. (ref. 72); ▲, VanHeijningen, et al. (ref 70); ♦, Hogervorst (ref. 73); ⧗, Schafer, et al. (ref. 74); #, Durbin, et al. (ref. 75); *, Srivastava, et al. (ref. 66).

to determine D_{12}. Hogervorst's data are approximately 5% lower than the present results, and further study will be made of the system in order to elucidate the discrepancy. Table 6 lists the present results for krypton-argon.

Table 6 - DIFFUSION COEFFICIENT MEASUREMENTS COREECTED TO 1 ATMOSPHERE PRESSURE FOR Kr-Ar

Temperature (°K)	D_{12} (cm^3/sec)
599.8	0.503
821.3	0.882
1008.0	1.26
1008.7	1.27
1010.4	1.27

Thermal diffusion factors for Ne-Ar

W. L. Taylor

In a previous report [77] thermal diffusion factors, α_T, were reported for the Ne-Ar system. The feed mixtures for these experiments were made from commercial research grade gases containing the naturally occurring isotopic abundance of masses 20/21/22 and 36/38/40 for neon and argon, respectively. The common isotope of neon (~90%) possesses mass 20 and that of argon (~99-1/2%) possesses mass 40. Because the value of α_T is determined by mass spectrometric analysis of the separation obtained in samples taken at the end of an experiment, an inherent problem was encountered in accurate determination of the neon/argon ratio due to the coincidence of the singly ionized neon and doubly ionized argon peaks. Calibration of the mass spectrometer with the pure gases was made to compensate for this fact but, with the probable exception of the two high temperature points which were analyzed on a different machine, this calibration was inaccurate. Fortunately the analytical results were available and it was possible to reanalyze the separation on the basis of the neon and argon peaks for most cases. In several cases the experimental uncertainties in this procedure were unacceptably high, and the experiments were rerun using ^{22}Ne/Ar feed mixtures. The revised results are given in Table 7 where, because other workers reported using neon of naturally occurring isotopic abundances, the following mass correction was made for comparison:

$$\alpha_T(\text{mass } 20/\text{mass } 40) = \frac{M_i - M_k}{M_i + M_k} \frac{M_i + M_j}{M_i - M_j} \times \alpha_T(\text{mass } 22/\text{mass } 40)$$

where M_i = mass 40, M_j = mass 22, and M_i = mass 20. No correction was made for the less than 10% neon occurring in natural abundance neon.

Table 7 - α_T FOR THE Ne-Ar SYSTEM AT 250°K

x^a (Feed)	α_T	% Dev
0.107	0.137	3.6
0.358	0.147	-2.2
0.516	0.153	-7.0
0.699	0.193	4.5
0.903	0.219	2.4

α_T for an Equimolar Mixture of Ne-Ar

Temp (°K)	α_T	Est. Unc. (±%)
250	0.151[b]	4.0
351	0.187	6.9
450	0.188	3.6
551	0.194	9.0
650	0.190	5.7
750	0.190	13.9

[a] Mole fraction of neon.

[b] Computed from least squares fit to the data above.

The composition dependence is shown in Figure 21 and the temperature dependence in shown in Figure 22. The reciprocal thermal diffusion factor (solid circles in Figure 21) were fitted to a linear equation by the method of least squares, which resulted in the equation

$$1/\alpha_T = - 3.63\ X_{Ne} + 7.95$$

where X_{Ne} is the mole fraction of neon in the mixture. The dashed curves in Figures 21 and 22 are theoretical calculations with the Dymond-Alder [78] potential with parameters given by Lin and Robinson [79]. As can be seen from the figures, the experimental data cluster very nicely around the theoretical curve and it is unlikely that much improvement could be made to the potential form or parameters based on the existing data.

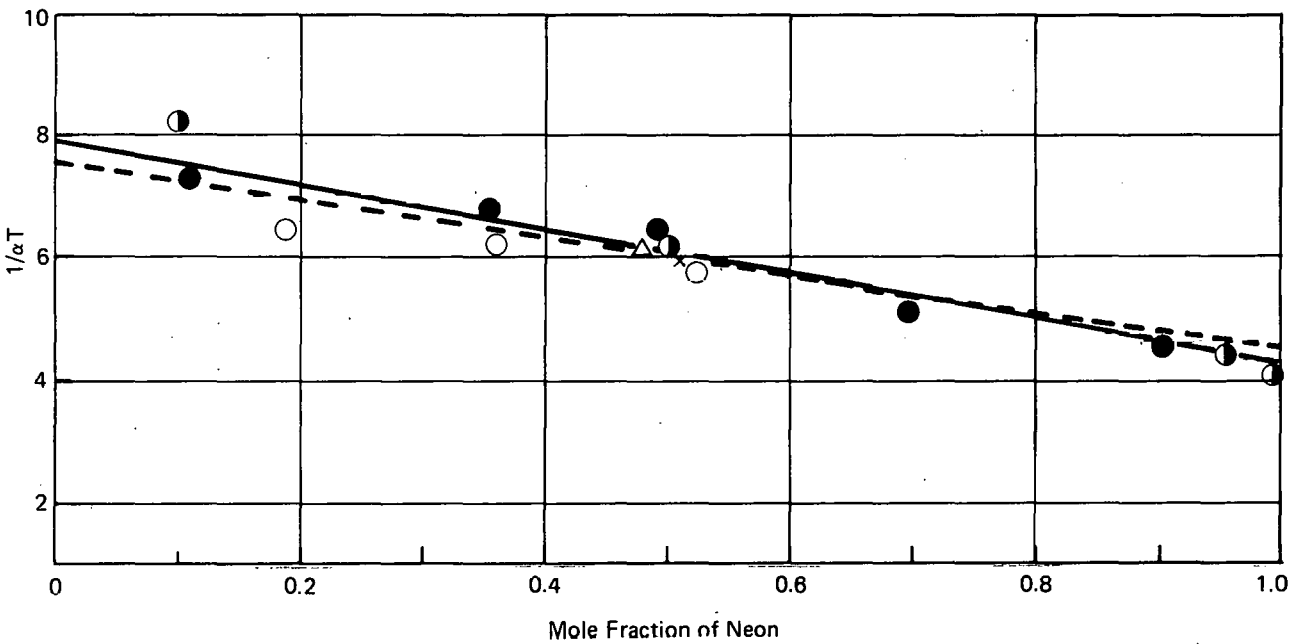

FIGURE 21 - Composition dependence of the reciprocal of the thermal diffusion factor for Ne-Ar at 250°K. The experimental points are: ●, present data; ◑, Grew, et al. (ref. 80); ○, Ibbs, et al. (ref. 81); △, Grew, et al. (ref 82); and X, Grew, et al. (ref 83). The solid line is the least-square linear fit to the present data and the dashed curve is the theoretical calculation of $[\alpha_T]_3$ using the Dymond-Alder potential.

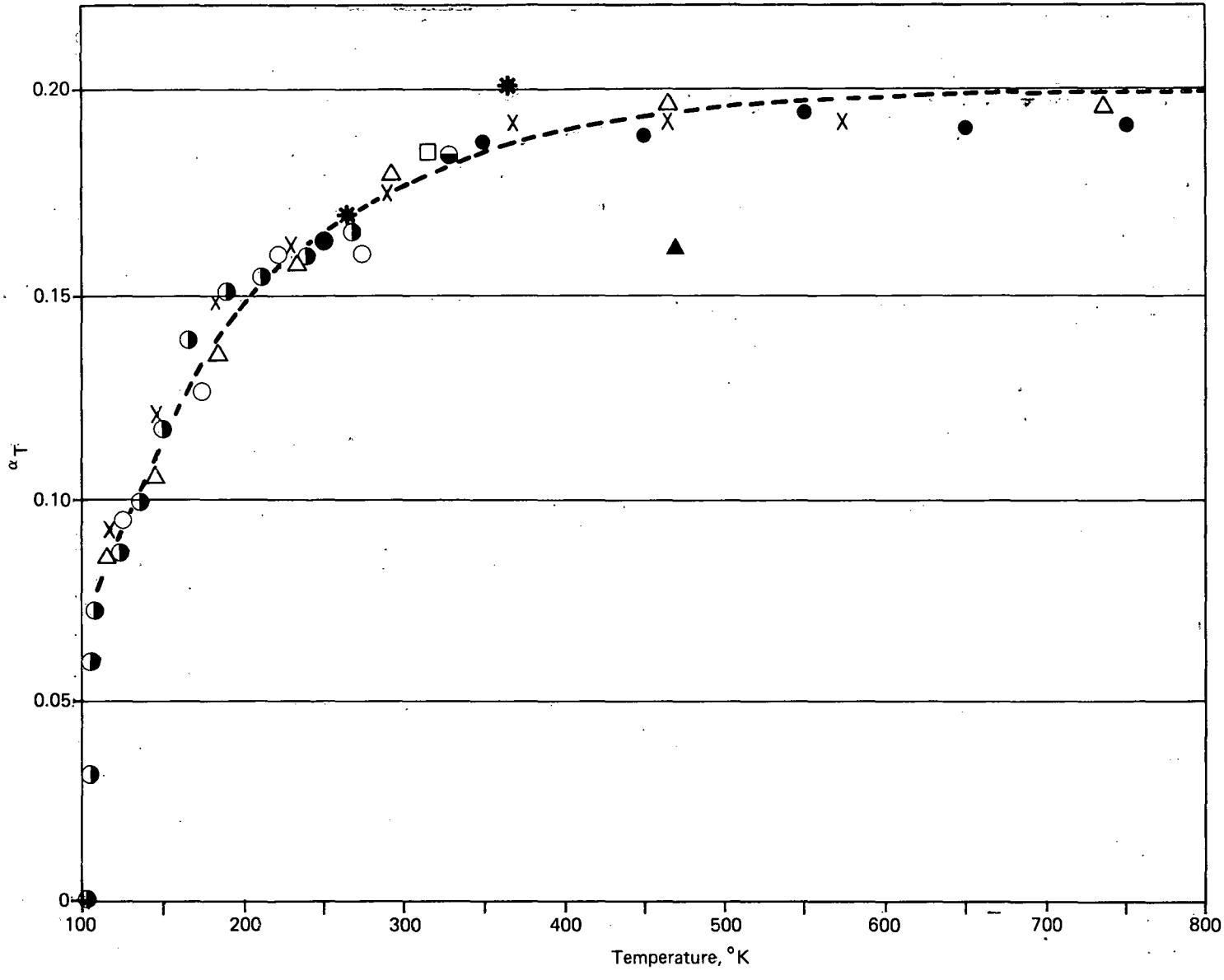

FIGURE 22 - Temperature dependence of the thermal diffusion factor of equimolar Ne-Ar. The symbols have the same meaning as in Figure 21 with the additon of: □, Saxena, et al. (ref. 84); ◒, Atkins, et al. (ref. 85); ▲, Laranjiera, et al. (ref. 86); and *, Drickamer, et al. (ref. 87).

References

1. Mound Laboratory Activities for the Division of Physical Research: January-June 1976, MLM-2354 (Sept. 30, 1976), pp. 22-25.

2. Mound Laboratory Activities in Chemical and Physical Research: July-December 1976, MLM-2414 (May 4, 1977), pp. 11-12.

3. Mound Laboratory Activities in Chemical and Physical Research: January-June 1977, MLM-2450 (Oct. 4, 1977), pp. 21-22.

4. A. Schmolz and F. Noack, Ber. Bunseges. Physik. Chem., 78, 339 (1974).

5. B. Nowak, N. Pišlewski, and W. Leszcyński, Phys. Stat. Sol. (a), 37, 669 (1976).

6. O. T. Malutchkox, J. J. Lileeva, and A. A. Tchertkov, in Proceedings of International Congress on Hydrogen in Metals, Paris, 1972, p. 261.

7. E. Lebsanft, G. Arnold, K. H. Klatt, M. A. Pick, J. Töpler, and H. Wenzl, Proceedings of Second International Congress on Hydrogen in Metals, Paris, June 1977, paper 1E10.

8. K. Yamanaka, H. Saito and M. Someno, Nippon Kagaku Kaish: 8, 1267 (1975).

9. J. J. Reilly and R. Johnson, in Proceedings of 1st World Hydrogen Energy Conference, Miami Beach, March 1976, Vol. II, 8B-3.

10. H. Buchner, M. A. Gutjahr, K. D. Beccu and H. Säufferer, Z. Metallkunde, 63, 497 (1972).

11. Mound Laboratory Activities in Chemical and Physical Research: January-June 1977, MLM-2450 (Oct. 4, 1977), pp. 22-26.

12. C. Korn and D. Zamir, J. Phys. Chem. Solids, 34, 725 (1973).

13. Mound Laboratory Activities for the Division of Physical Research: January-June 1975, MLM-2241 (Nov. 11, 1975), pp. 20-24.

14. D. G. Westlake, S. T. Ockers, and W. R. Gray, Met. Trans., 1, 1361 (1970).

15. K. I. Hardcastle and T. R. P. Gibb, Jr., J. Phys. Chem., 76, 927 (1972).

16. J. M. Rowe, Sol. State Comm., 11, 1299 (1972).

17. D. G. Westlake, M. H. Mueller, and H. W. Knott, J. Appl. Cryst., 6, 206 (1973).

18. H. Asano and M. Hirabayashi, Phys. Stat. Sol. (a), 15, 267 (1973).

19. R. R. Arons, H. G. Bohn, and H. Lütgemeier, J. Phys. Chem. Solids, 35, 207 (1974).

20. G. L. Silver, Plutonium in Natural Waters, MLM-1870 (Dec. 16, 1971), 15 pp.

21. G. L. Silver, Radiochem. Radioanal. Letters, 9 (5-6), 315 (1972).

22. A. Ringbom, Complexation in Analytical Chemistry, Interscience Publishers, 1963, p. 352.

23. A. Ringbom, op. cit., p. 38.

24. T. M. Florence and G. E. Batley, Talanta, 24, 151 (1977).

25. W. L. Polzer, "Solubility of Plutonium in Soil/Water Environments", in Rocky Flats Symposium on Safety in Plutonium Handling Facilities, CONF 710401 (April 13, 1971), p. 411.

26. J. H. Patterson, G. B. Nelson, and G. M. Matlack, The Dissolution of 238-Pu in Environmental and Biological Systems, LA-5624 (July 1974), 6 pp.

27. G. L. Silver, in Mound Laboratory Activities in Chemical and Physical Research: January-June 1977, MLM-2450 (Oct. 4, 1977), pp. 33-34.

28. R. M. Garrels and C. L. Christ, Solutions, Minerals, and Equilibria, Harper and Row Publishers, New York, 1965, pp. 129-139.

29. E. Whittaker and G. Robinson, The Calculus of Observations, Dover Publications, Inc., New York, 1967, p. 368.

30. G. L. Silver, Non-Euclidean Simplex Optimization, MLM-2427 (August 15, 1977), 30 pp.

31. C. E. Van Orstrand, Philosophical Magazine, 19(6), 366 (1910).

32. I. Todhunter, Theory of Equations, Macmillan and Company, London, 1867, p. 206.

33. M. Merriman, in Higher Mathematics, M. Merriman and R. Woodward (eds.), John Wiley and Sons, New York, 1896, p. 28.

34. G. L. Silver, in Mound Laboratory Activities for the Division of Physical Research: July-December 1974, MLM-2198 (April 10, 1975), p. 32.

35. G. L. Silver, in Mound Laboratory Activities for the Division of Physical Research: July-December 1975, MLM-2296 (May 14, 1976), p. 24.

36. G. L. Silver, in Mound Laboratory Activities for the Division of Physical Research: January-June 1976, MLM-2354 (September 30, 1976), pp. 26-27.

37. G. L. Silver, in Mound Laboratory Activities in Chemical and Physical Research: January-June 1977, MLM-2450 (Oct. 4, 1977), pp. 33-35.

38. Mound Laboratory Activities for the Division of Physical Research: July-December 1975, MLM-2296 (May 14, 1976), pp. 40-41.

39. Mound Laboratory Activities for the Division of Physical Research: January-June 1976, MLM-2354 (Sept. 30, 1976), pp. 32-35.

40. Mound Laboratory Activities for the Division of Physical Research: July-December 1972, MLM-2013 (February 14, 1973), pp. 56-59.

41. Mound Laboratory Activities for the Division of Physical Research: January-June 1977, MLM-2450 (October 4, 1977), p. 38.

42. Mound Laboratory Activities for the Division of Physical Research: January-June 1976, MLM-2354 (September 30, 1976), pp. 35-36.

43. D. E. Horner, C. F. Coleman, Plutonium Extraction from Nitrate and Sulfate Solutions by Amines and Organophosphorous Compounds, ORNL-3051 (March 9, 1961).

44. C. A. Blake, Jr., A. T. Gresky, J. M. Schmitt, R. G. Mansfield, Comparison of Dialkyl Phenylphosphonates with Tri-n -Butyl Phosphate in Nitrate Systems: Extraction Properties, Stability, and Effect of Diluent on the Recovery of Uranium and Thorium from Spent Fuels, ORNL-3374 (January 23, 1963).

45. M. R. Hertz, W. S. Stringham, R. M. Watrous, A Solvent Extraction Method for the Recovery of Thorium-229 from Aged Uranium-233, MLM-2151 (January 31, 1975).

46. Mound Laboratory Activities in Chemical and Physical Research: July-December 1976, MLM-2414 (May 4, 1977), p. 21.

47. M. Jakob, Heat Transfer, Vol I, Wiley, New York, 1949, p. 551.

48. A. E. Dukler, Chem. Eng. Progress, 55, 62 (1959).

49. W. M. Rutherford, J. Chem. Phys., 59, 6061 (1973).

50. G. A. DuBro, Measurements of Gaseous Diffusion Coefficients by a Modified Two-Bulb Method, MLM-1635 (April 1969), 165 pp.

51. S. Weissman and G. A. DuBro in Proceedings of the Fifth Symposium on Thermophysical Properties, American Society for Mechanical Engineers, New York, 1970, pp. 78-83.

52. G. A. DuBro and S. Weissman, Phys. Fluids, 13, 2682 (1970).

53. G. A. Dubro and S. Weissman, Phys. Fluids, 13, 2689 (1970).

54. S. Weissman and G. A. DuBro, J. Chem. Phys., 54, 1881 (1971).

55. S. Weissman, J. Chem. Phys., 55, 5839 (1971).

56. S. Weissman, Phys. Fluids, 16, 1425 (1973).

57. S. Weissman, Phys. Fluids, 17, 254 (1974).

58. E. P. Ney and F. C. Armistead, Phys. Rev., 71, 14 (1947).

59. R. D. Present, Kinetic Theory of Gases, McGraw-Hill Book Co. New York (1958).

60. W. Jost, Diffusion in Solids, Liquids, Gases, Academic Press, Inc., New York (1960).

61. R. Paul, Phys. Fluids, 3, 905 (1960).

62. Maxwell, Electricity and Magnetism, Oxford University Press, London (1892).

63. Lord Rayleigh, Theory of Sound II, The MacMillan Company, New York (1878).

64. J. O. Hirschfelder, C. F. Curtiss, and R. B. Bird, Molecular Theory of Gases and Liquids, John Wiley & Sons, Inc., New York (1954).

65. A. P. Malinauskas, J. Chem. Phys., 45, 4704 (1966).

66. B. N. Srivastava and K. P. Strivastava, J. Chem. Phys., 30, 984 (1959).

67. B. P. Mathur, PhD Thesis, University of Rajasthan, Jaipur, India (1967).

68. B. P. Mathur and S. C. Saxena, J. Appl. Sci. Res., 18, 325 (1968).

69. H. Watts, Trans. Faraday Soc., 60, 1745 (1964).

70. R. J. J. vanHeijningen, J. P. Harpe and J. J. M. Beenakker, Physica, 38, 1 (1968).

71. A. E. Loiko, B. A. Ivakin and P. E. Suetin, Sov. Phys.-Tech. Phys., 19, 434 (1974).

72. A. E. Loiko, B. A. Ivakin and P. E. Suetin, Sov. Phys.-Tech. Phys., 18, 266 (1973).

73. W. Hogervorst, Physica, 51, 59 (1971).

74. K. Schafer and K. Schuhman, Z. Elektrochem. 61, 246 (1957).

75. L. Durbin and R. Kobayashi, J. Chem. Phys., 37, 1643 (1962).

76. L. Miller and P. C. Carman, Trans. Faraday Soc., 57, 2143 (1964).

77. Mound Laboratory Activities for the Division of Physical Research: July-December 1975, MLM-2296 (May 14, 1976), p. 52.

78. J. H. Dymond and B. J. Alder, J. Chem. Phys., 51, 309 (1969).

79. H. M. Lin and R. L. Robinson, Jr., J. Chem. Phys., 54, 52 (1970).

80. K. E. Grew and W. A. Wakeham, J. Phys. B: Atom. Mol. Phys., 4, 1548 (1971).

81. T. L. Ibbs and K. E. Grew, Proc. Phys. Phys. Soc., 43, 142 (1931).

82. K. E. Grew, F. A. Johnson, and W. E. J. Neal, Proc. Roy. Soc., A224, 513 (1954).

83. K. E. Grew, Proc. Roy. Soc. (London), A189, 402 (1947).

84. V. K. Saxena, V. P. S. Nain, and S. C. Saxena, J. Chem. Phys., 48, 3681 (1968).

85. B. E. Atkins, R. E. Bastick, and T. L. Ibbs, Proc. Roy. Soc. (London), A172, 142 (1939).

86. M. F. Laranjiera and J. Kistemaker, Physica, 26, 431 (1960).

87. H. G. Drickamer and J. R. Hofto, J. Chem. Phys., 17, 1165 (1949).

Distribution

EXTERNAL

Technical Report Library, Monsanto, St. Louis

TID-4500, UC-4 and 22 (240)

R. M. Munson, DOE/Dayton Area Office
R. B. Craner, Sandia Laboratories Albuquerque
R. K. Flitcraft, Monsanto Research Corporation
W. J. Haubach, DOE/ Division of Basic Energy Sciences
N. Haberman, DOE/Division of Nuclear Research and Application
W. E. Moddeman, University of Dayton
F. D. Stevenson, DOE/Division of Basic Energy Sciences
C. P. Sutter/R. N. Diebel, Atlantic Richfield
D. White, University of Pennsylvania
R. N. Zare, Columbia University

INTERNAL

A. Attalla
V. L. Avona
R. C. Bowman, Jr.
W. T. Cave
R. J. DeSando
R. E. Eppley
C. W. Huntington
B. E. Jepson
L. V. Jones
K. C. Jordan
B. R. Kokenge
C. M. Love
J. R. McClain
E. D. Michaels
W. J. Roos
W. M. Rutherford
R. A. Schwind
G. L. Silver
W. L. Taylor
R. E. Vallee
R. M. Watrous
Document Control
Library (15)
Publications (25)